INLETS FILE

DECLASSIFIED

CONFIDENTIAL

Copy 93
RM L57K14

NACA RM L57K14

NACA CASE FILE COPY

RESEARCH MEMORANDUM

INVESTIGATION OF FIXED-GEOMETRY SUPERSONIC INLETS WITH BYPASS DUCTS FOR MATCHING TURBOJET-ENGINE AIR-FLOW REQUIREMENTS OVER A RANGE OF TRANSONIC AND SUPERSONIC SPEEDS

By Abraham Leiss and Walter L. Kouyoumjian

Langley Aeronautical Laboratory
Langley Field, Va.

CLASSIFICATION CHANGED TO
DECLASSIFIED AUTHORITY
NTP JULY 1959 - JUNE 1960

CLASSIFIED DOCUMENT

This material contains information affecting the National Defense of the United States within the meaning of the espionage laws, Title 18, U.S.C., Secs. 793 and 794, the transmission or revelation of which in any manner to an unauthorized person is prohibited by law.

NATIONAL ADVISORY COMMITTEE FOR AERONAUTICS

WASHINGTON
February 3, 1958

T58-3252

CONFIDENTIAL

NATIONAL ADVISORY COMMITTEE FOR AERONAUTICS

RESEARCH MEMORANDUM

INVESTIGATION OF FIXED-GEOMETRY SUPERSONIC INLETS WITH BYPASS DUCTS FOR MATCHING TURBOJET-ENGINE AIR-FLOW REQUIREMENTS OVER A RANGE OF TRANSONIC AND SUPERSONIC SPEEDS

By Abraham Leiss and Walter L. Kouyoumjian

SUMMARY

A method for matching fixed-geometry supersonic-inlet air flow and turbojet-engine air-flow requirements by means of a bypass duct was investigated. This investigation consisted of ground and flight tests. The experimental mass-flow ratios and total-pressure recovery were determined by the ground tests which included a Mach number range from 0.96 to 2.03 and a Reynolds number range of 3.98×10^6 to 8.41×10^6. The flight tests were made to determine the effect of an inlet bypass duct on the zero-lift drag characteristics of the inlet models at transonic and supersonic speeds. Two bypasses were tested, a 360° annular bypass and twin bypass segments with slots. The flight tests covered a Mach number range from 0.8 to 1.95 and a Reynolds number range, based on maximum body diameter, from 2×10^5 to 8×10^5. The results indicated that the use of a bypass on a fixed-geometry inlet allows the required engine-air mass flow to be matched over a larger Mach number range. However, the models with bypass had slightly higher external drags throughout the flight Mach number range than the inlet without a bypass.

INTRODUCTION

One of the problems facing designers of supersonic airplanes, employing air-breathing engines, has been the successful matching of the inlet mass flow with the engine-air mass-flow requirements throughout the flight Mach number range without introducing prohibitive drag penalties. In general, designing a fixed-geometry inlet suitable for a turbojet engine at subsonic speeds results in an excess inlet area at

supersonic speeds; and hence air spillage, which results in a severe drag penalty, occurs. Also, proper sizing of the inlet at supersonic speeds results in starving the engine at subsonic speeds with a resultant severe loss in engine thrust.

One proposed solution to the inlet engine matching problem, in conjunction with a fixed-geometry inlet, is the use of an auxiliary exit system located in the subsonic diffuser section upstream of the turbojet compressor. This exit system would be used to bypass the excess air supplied by the inlet at supersonic speeds above the design Mach number. Performance tests of similar systems are presented in references 1 to 4. These reference data indicate that spillage rates as high as 23 percent can be achieved by using a bypass with only a fraction of the drag increase that resulted when this spillage was taken around the inlet leading edge through a normal shock.

Reference 5 presents a comparison of engine performance employing translating spike and fixed geometry with bypass inlets. This reference indicates favorable gains in pressure recovery for the bypass over the others listed. The main disadvantage to the bypass systems previously tested was the added weight penalties, due to the additional mechanism needed to regulate the bypass spillage area. In an attempt to eliminate this control mechanism and simplify the inlet, the Langley Pilotless Aircraft Research Division has conducted tests to investigate a bypass method that would match the engine air-flow requirements exactly at two Mach numbers and practicably match the engine air-flow requirements at intermediate speeds. This paper presents the results of a preliminary investigation of this method.

Two supersonic inlets, each with a bypass, were tested and compared with a fixed-geometry inlet without bypass. Each of the three models used a conical shock with a 50° cone, designed for Mach number 2.0, and each inlet was mounted on identical afterbody and fin configurations. The design theory of the two bypass models tested is also presented. Drag data are presented over a Mach number range from 0.8 to 1.95 and a Reynolds number range (based on maximum body diameter) of 2×10^5 to 8×10^5. These models were tested at the Langley Pilotless Aircraft Research Station at Wallops Island, Va.

SYMBOLS

a	tangential acceleration, ft/sec^2
A	area, sq in.

A_o	stream tube area, sq in.
C_D	drag coefficient, D/qA_f
d	diameter, in.
D	drag, lb
g	acceleration due to gravity, ft/sec^2
L	nozzle minimum length, in.
M	Mach number
N_{Re}	Reynolds number based on maximum body diameter
p	static pressure, lb/sq ft
p_t	total pressure, lb/sq ft
q	dynamic pressure, lb/sq ft
R	stream tube-area ratio at two Mach numbers, $A_{o,i,2}/A_{o,i,1}$, $A_{o,B,2}/A_{o,B,1}$, $A_{o,e,2}/A_{o,e,1}$, or $A_{o,N,2}/A_{o,N,1}$
R'	stream tube-area ratio at $M_{\infty,1} = 1.0$
v	velocity, ft/sec
w	mass flow, lb/sec
W	weight, lb
w/w_∞	ratio of mass flow of air through the duct to mass flow of air through a free-stream tube of air equal to inlet area defined by lip diameter
x	distance from tunnel exit to cowling lip, in.
γ	flight-path angle, deg
ρ	density, slugs/cu ft

Subscripts:

b	base
B	bypass
B'	bypass entrance
c	center body at lip leading-edge station
e	cowling exit at nozzle entrance
f	frontal
i	cowling inlet at lip leading edge
N	engine requirements
s	slots
T	total
x	external
X	bypass exit
∞	free stream
1,2	design conditions (two different Mach numbers)

INLET DESIGN

The inclusion of a bypass system to provide a means of spilling the excess air supplied by the fixed-geometry inlet adds another variable to the inlet engine matching problem. Thus, by properly sizing the inlet and bypass relative to the engine requirements, a fixed-geometry system can be designed that will match the engine air-flow requirements exactly at two specified Mach numbers. It appears further that a reasonably close matching of the engine air-flow requirements may occur over the intermediate range of Mach numbers.

The following method was used for determining the required size of inlet and bypass exit at two Mach numbers.

In terms of the free-stream tube area (i.e., the mass flow required to satisfy the continuity relation),

$$A_{o,i} = A_{o,N} + A_{o,B} \tag{1}$$

and since $R = \frac{A_{o,2}}{A_{o,1}}$, then

$$R_i\left(A_{o,i}\right)_1 = R_N\left(A_{o,N}\right)_1 + R_B\left(A_{o,B}\right)_1 \tag{2}$$

and when equation is simplified

$$\left(A_{o,i}\right)_1\left(R_i - R_B\right) = \left(A_{o,N}\right)_1\left(R_N - R_B\right) \tag{3}$$

note that

$$A_{o,i} = \frac{A_{o,i}}{A_i}\left(A_i\right)$$

where

$$\frac{\left(A_{o,i}\right)_1}{A_i} = \left(\frac{w_i}{w_\infty}\right)_1 \tag{4}$$

and the required inlet area is

$$A_i = \frac{\left(A_{o,N}\right)_1}{\left(\frac{w_i}{w_\infty}\right)_1}\left(\frac{R_N - R_B}{R_i - R_B}\right) \tag{5}$$

The corresponding bypass exit area required is obtained from equation (1) and is given as follows:

$$A_B = \frac{\left(A_{o,i}\right)_1 - \left(A_{o,N}\right)_1}{\left(\frac{A_{o,B}}{A_B}\right)_1} \tag{6}$$

In equation (6) the term $\left(\frac{A_{o,B}}{A_B}\right)$ is equivalent to the mass-flow ratio out of the bypass and is based on the bypass exit area, that is,

$$\left(\frac{A_{o,B}}{A_B}\right)_1 = \left(\frac{\rho_B v_B A_B}{\rho_\infty v_\infty A_B}\right)_1 = \left(\frac{\rho_B v_B}{\rho_\infty v_\infty}\right)_1 \tag{7}$$

In the present paper, the two Mach numbers selected for design were 1.0 and 2.0. A conical shock inlet and a sonic bypass were matched to the typical engine requirements selected.

By using the weight flow and engine inlet area of this typical engine, $A_{o,N}$ is determined from the following equation:

$$\frac{A_{o,N}}{A_N} = \frac{w_N}{w_\infty} \tag{8}$$

Then from equation (5), A_i may be computed in terms of R. Typical regulation curves are shown in figure 1 for a typical turbojet engine, a conical shock inlet, and a sonic bypass system. From these curves the values of R' (ratio of capture area at flight Mach numbers and capture area at a free-stream Mach number of 1) for the inlet, bypass, and engine can be read up to a Mach number of 2.0. Figure 1 also presents the variation of the total-pressure recovery used to compute R_N.

Note that R_i represents the air-flow characteristics of a 25° half-angle conical inlet designed for a mass-flow ratio $\left(\frac{w_i}{w_\infty}\right)$ of 1.0 at $M_\infty = 2.0$ and with $\frac{A_i - A_c}{A_i} = 0.74$; R_N represents the mass-flow characteristics of a turbojet engine for the total-pressure recoveries presented in figure 1; and R_B represents the conical-shock, normal-shock loss with a theoretical 98-percent pressure recovery through the sonic bypass.

By using these expressions, the capture area and bypass area can be determined. In figure 1 at $M_\infty = 2.0$ (which is matched for $M_\infty = 1$),

$$R'_B = 1.50$$

$$R'_i = 1.35$$

$$R'_N = 1.18$$

By using $(w_i/w_\infty)_1 = 0.74$ as characteristic of the selected inlet where

$$\left(\frac{w_i}{w_\infty}\right)_1 = \frac{A_i - A_c}{A_i} \qquad (M_\infty = 1.0) \tag{9}$$

and by substituting these values into equation (5), the following equation is obtained:

$$A_i = 2.88\left(A_{o,N}\right)_1 \tag{10}$$

This results in a large inlet capture area. To obtain a physical system with reduced inlet area requires a system that can vary the amount of air bypassed at two selected Mach numbers. This can possibly be achieved by the use of slots. At $M_\infty < 1.0$ the pressure difference across the slots will be small, while at supersonic speeds the pressure difference increases until the slots are choked. This increases the bypass mass-flow ratio with increasing Mach number. By designing for half of the necessary spillage through the slots at $M = 2.0$, R_B effectively increases from 1.50 to 3.00. (The actual area of the slots used was determined for an assumed orifice coefficient of 0.50.) Substituting this new value of R_B into equation (5) yields

$$A_i = 1.49\left(A_{o,N}\right)_1 \tag{11}$$

Thus, the inlet area required in this case is approximately one-half of that required for the first case discussed.

MODELS AND APPARATUS

Flight Models

Sketches and photographs of the models are shown in figures 2 to 6. Three models (designated as models A, B, and C) were designed with conical shock inlets, cylindrical 7-inch-diameter center sections with fineness ratios of 3.5; 4° conical boattails with fineness ratios of 1.26; and

four 60° delta fins of total aspect ratio 2.35 per plane. The length of the afterbody was the same for the three models (fig. 2), but the overall length of the models differed slightly since the three cowlings varied slightly in length.

Inlet and Bypass Geometry

The inlet and bypass information for the three models is given in table I and illustrated in figure 3. The three inlets had 25° half-angle conical center bodies, 11° external lip angles, 4° internal lip angles, and 42.5° cowling to lip angles.

Model A had a conventional conical shock inlet, designed for Mach number 2.0, incorporated no bypass, and had a subsonic diffuser ratio $\left(\frac{A_e}{A_i}\right)$ of 0.790. The center body of model A was supported in the cowling by three equally spaced struts.

Model B had a 360° annular bypass and was designed by using equation (10) and the method described in the section entitled "Inlet Design." The subsonic diffuser ratio was 0.414. The center body of model B was supported in the cowling by four equally spaced struts.

Model C was designed with a reduced inlet capture area. Therefore, the amount of bypass mass-flow ratio necessary to match the turbojet-engine requirements was reduced. This model was designed by using equation (11) and has about one-third the proportional bypass area as model B. The total bypass area was divided into two components, slots and annular segments. (See fig. 3.) Model C had a subsonic diffuser ratio of 0.726.

Ground-Test Models

Models B and C were preflight tested in the Langley preflight jet of the Pilotless Aircraft Research Station at Wallops Island, Va. (See ref. 6.) For these tests, the model tail cone with fins was replaced by a similar tail cone without fins and was mounted in a test stand as shown in figure 4. The test tail cone had the same internal geometry as the original tail cones and also had provision for installing exits of different areas. The ground-test model and the five different exits (2.917, 3.450, 3.688, 3.912, and 4.125 in. in diameter) tested are shown in figure 5. Table II summarizes the 40 ground tests made on models B and C.

INSTRUMENTATION

Ground Tests

Included in figure 5 is the test-cone instrumentation. Installed ahead of the exit nozzle were 13 total-pressure tubes equally spaced in 180° of the cone cross section and 1 slotted integrating rake along one-half of the cone cross-section center line. All of the total-pressure orifices were in the same vertical plane, 8.37 inches ahead of the exit. The total- and static-pressure tubes shown in figure 3 were installed for the ground-test measurements and disconnected for the test flights.

Model B had a manifold total-pressure rake at the bypass entrance and a static-pressure orifice in the bypass duct. Model C also had this instrumentation with an additional static- and total-pressure orifice at the exit of the bypass.

All the model pressure readings were recorded with six-cell manometer-type instruments. The free-stream conditions were recorded by electrical pressure recorders of the strain-gage type. A 10-cycle-per-second timer correlated all time histories on recording paper. Shadowgraphs, which were photographed at an exposure of approximately 0.003 second, were obtained by using a carbon-arc light source and a translucent glass screen.

Flight Tests

The three flight models were propelled to supersonic speeds by single Deacon booster rocket motors each equipped with four stabilizing fins (fig. 6). The models were launched at an elevation angle of 60° and followed a zero-lift trajectory at 0° angle of attack. The models were flight tested at the Pilotless Aircraft Research Station at Wallops Island, Va.

Velocity and Mach number of the test models were obtained by the use of continuous wave Doppler radar. The trajectories of the models were obtained by NACA modified SCR-584 tracking radar. Atmospheric data and wind characteristics for each flight were obtained by means of a balloon carrying a Rawinsonde sent aloft at the time of each flight. Total-drag data were obtained during the decelerating portion of the flight, after drag separation of the booster from the model. The total drag was evaluated by using the expression

$$C_D = -\frac{W}{gqA_f}(a + g \sin \gamma) \tag{12}$$

where a was obtained by differentiating the velocity-time curve from Doppler radar. The values of q and γ were obtained from measurements of tangential velocity and atmospheric conditions along each trajectory.

Accuracy

The accuracy of the data is estimated to be within the following limits:

w/w_∞	±0.02
C_D	±0.01
M	±0.01

RESULTS AND DISCUSSION

Ground Test

In order to evaluate the individual inlet characteristics of the air mass flow and total-pressure recovery, pressure measurements were taken and the data were computed by the method outlined in the appendix. The 40 ground tests covered a range of Reynolds number from 3.98×10^6 to 8.41×10^6 and a range of Mach number from 0.96 to 2.03 (based on maximum body diameter).

Mass-flow ratio.- Presented in figure 7 are the mass-flow characteristics for models B and C as a function of mass-flow ratio $\left(\frac{w_e}{w_\infty}\right)$ passing through the model for each free-stream Mach number tested. Model B operated at a capture mass-flow ratio of 1.0 for $M_\infty = 2.03$ and at a capture mass-flow ratio of 0.74 for $M_\infty = 1.17$. Also the bypass configuration for inlet B passes a relatively high proportion of the total inlet mass-flow ratio $\left(\frac{w_T}{w_\infty}\right)$. The amount of bypass mass-flow ratio $\left(\frac{w_{B'}}{w_\infty}\right)$ ranges from 50 percent to 60 percent of the total capture mass-flow ratio for the test Mach number range.

The bypass mass-flow ratio for model C (fig. 7) is the sum of the mass-flow ratio passing through the bypass annular segment plus the mass flow passing through the slots cut into the cowling of the bypass duct and is defined as follows:

$$\left(\frac{w_{B'}}{w_\infty} = \frac{w_s}{w_\infty} + \frac{w_X}{w_\infty}\right) \tag{13}$$

The bypass mass-flow ratio for model C ranges only from 10 percent to 19 percent of the total capture mass-flow ratio through the test Mach number range. The curves in figure 7 indicate that the bypass duct for both models is operating with a sonic minimum station in each bypass duct. The amount of inlet bypass mass flow for a choked bypass duct is dependent on the minimum area and duct total pressure. The relatively little variation of bypass mass-flow ratio with increasing engine mass-flow ratio indicates a choking condition in the bypass.

Figure 8 presents the variation of mass-flow-ratio components as a function of free-stream Mach number for models B and C. The air mass-flow ratio through the bypass and exits was calculated from the measured pressures. The inlet or total air mass-flow ratios were assumed to be the total of the exit and bypass air mass-flow ratios.

Presented in figure 8(a) is the inlet design curve for model B. Since $(w_i/w_\infty)_1 = 0.74$ which is equal to $(A_i - A_c)/A_i$ at $M_\infty = 1.0$, then

$$(w_i/w_\infty)_2 = R'_{i,2}(A_i - A_o)/A_i \tag{14}$$

for all free-stream Mach numbers. The values of $R_{i,2}$ for each free-stream Mach number were obtained from figure 1. Note that the inlet air mass-flow ratio (w_T/w_∞), experimental results using exit V, closely matches the inlet design curve. The measured exit air mass-flow ratio (□), using exit V, is higher than the design engine air mass-flow ratios for equivalent total-pressure recoveries. Therefore, the bypass for this exit was undersized. However, when exit III was installed in the ground-test model the exit air mass-flow ratios (△) and the design engine air mass-flow ratios, for equivalent total-pressure recoveries, were in close agreement. However, the inlet air mass-flow ratio with this exit was lower than the design inlet air mass-flow ratio. Therefore, a slightly smaller inlet or a slightly larger bypass would have permitted the flow through the bypass to be equivalent to the design bypass air mass-flow ratio and spillage eliminated.

The required curve for the engine air mass-flow ratio for model B was computed by using figure 1 where,

$$w_T/w_\infty = w_e/w_\infty = R_{N,2}\left(\frac{A_{o,N}}{A_i}\right)_1 \tag{15}$$

The required bypass air mass-flow ratio for model B was then obtained from equation (1) where

$$w_B/w_\infty = w_i/w_\infty - w_N/w_\infty = w_T/w_\infty - w_e/w_\infty \tag{16}$$

since the model exit air mass flow (w_e) has the same significance as the engine inlet air mass flow (w_N).

Figure 8(b) shows the required design curves as well as the test results of the air mass-flow ratios through the inlet, bypass, and exit of model C. The required design curves were computed by the same method used for model B except equation (11) was used instead of equation (10). The results for the design and experimental inlet air mass-flow ratio (exit V is used) are in good agreement. However with this same exit installed, the exit air mass flow (□), at equivalent total-pressure recoveries, did not meet the required engine air mass-flow ratios; and the bypass was slightly undersized since the air mass-flow ratio through the bypass (◇) was less than the design air mass-flow ratio through the bypass. With exit III installed, the conditions were about the same except that the inlet had a small amount of spillage.

The mass flow of air passing through the slots of model C did not increase with M_∞ as can be seen in figure 7 from the $\frac{w_s}{w_\infty}$ values. The slots did not perform, as described in the section entitled "Inlet Design," and this condition may be attributed to the incorrect assumption of the orifice coefficient.

Note that model C bypassed less than 14 percent of the total air mass-flow ratio while model B bypassed about 50 percent of the total air mass-flow ratio. Figure 8 also indicates that both inlet configurations (with proper size bypass) could provide a close approximation to a typical turbojet-engine air mass-flow requirement curve (fig. 1) over the entire speed range, as well as for the two Mach numbers for which this inlet was designed.

Since model A was not ground tested, the theoretical variations of air mass-flow ratio and exit total-pressure recovery with Mach number for model A with supercritical flow was obtained by the method of reference 7 and is presented in figure 9. Reference 7 shows that for inlets similar to model A, the method of calculation used closely approximates the experimental results. By assuming an air mass-flow ratio of 1.0 and $M_e = 1.0$, a total-pressure recovery of 0.755 was computed at $M_\infty = 2.0$. A comparison of the air mass-flow ratios for models B and C with that computed for model A shows that the air mass-flow ratios were of the same order of magnitude at corresponding Mach numbers.

Pressure recovery.- Although models A, B, and C had similar total air mass-flow ratios (figs. 8 and 9) the bypass models (B and C) had less total-pressure recovery at corresponding total air mass-flow ratios. However, total-pressure recoveries, based on shock losses and exit weight flow (not exit air mass-flow ratio), would be approximately the same for the three models. For example, at a free-stream Mach number of 2.03 and at equivalent exit weight flows, $\frac{p_{t,e}}{p_{t,\infty}}$ was 0.68, 0.67, and 0.67 for models A, B, and C, respectively. The variations of the pressure recovery with exit air mass-flow ratios for the five exits tested with models B and C are presented in figure 10. The exit-total-pressure recovery, $\frac{p_{t,e}}{p_{t,\infty}}$, of the different models may be compared for identical engine mass flow (at each free-stream Mach number) by correcting w_∞ for the difference in A_i of the three models. Note that at a free-stream Mach number of 2.03 the maximum total-pressure recovery for model B was approximately 72.5 percent, while the maximum total-pressure recovery for model C was 75 percent.

Figure 10 shows that for models B and C the pressure recovery at supersonic speeds decreases as the exit air mass-flow ratio and the free-stream Mach number increases. The variation of pressure recovery as a function of exit air mass-flow ratio for model C appears to be more erratic than the variation of pressure recovery for model B.

Shown in figure 11 are shadowgraph pictures of models B and C with exit V which is the exit used on the models flight tested. It appears that model B operates critically at $M_\infty = 2.03$ (design Mach number) where the oblique shock from the cone is attached to the cowling lip. The experimental results, however, indicate supercritical operation.

Flight Tests

Figure 12 presents the variation in free-stream Mach number for the three models as a function of time. The three models were boosted to about $M_\infty = 2.0$ and coasted to about $M_\infty = 0.8$ in 13 seconds after firing. Figure 13 presents the Reynolds number variation (based on maximum body diameter) for the range of free-stream Mach numbers tested.

The internal drag for model A was calculated using the theoretical pressure recovery and mass-flow ratios shown in figure 9; whereas, the internal drags of models B and C were determined from the ground test data of figures 8 and 10. The method used for evaluating the internal drag is given in the appendix. The large contraction ratio, of about

3 to 1 from the maximum diameter station to the exit, and the cylindrical exit, of 1.05 diameters ahead of the exit, assured sonic rather than supersonic exit velocities and helped to provide uniform total and static pressures at the exit.

Figure 14 presents the total, internal, and external drag coefficients as a function of free-stream Mach number for the three inlets investigated. The difference between the model total drag coefficients, from the flight tests, and the internal drag coefficients was considered the external drag coefficients. The drag due to spillage about the cowling leading edge (although models B and C indicated little if any spillage (fig. 8)) and the drag due to the bypass mass flow remain included in the external drag.

The drag coefficient components for model A are presented in figure 14(a) and are considered as the reference data for the present series of inlets investigated. The internal drag coefficient of inlet models B and C are shown to be approximately the same at corresponding free-stream Mach numbers (fig. 14). The internal drag coefficient of model A, which was computed from theory, is shown to be slightly lower than the internal drag coefficients of models B and C throughout the flight Mach number range. However, the magnitudes of the internal drag coefficients are such that the relative levels of the external drag coefficients of the three models would not change, even if the average value of the internal drag coefficients were used.

Figure 15 presents a comparison of the measured experimental external drag coefficients. In order to present a more realistic comparison of the inlets, the external drag of model A was adjusted to allow for the necessary spillage to match the engine flow requirements. This corrected curve is indicated in figure 15 and the increase in external drag coefficient is due to the estimated spillage drag increments which would occur when the turbojet-engine air-flow requirements are matched at each flight Mach number. The spillage drag coefficients were obtained using the mass-flow curves of figures 8 and 9 and the data presented in references 5 and 7. Comparison of the curves for the experimental external drag coefficient and the corrected curve for the drag coefficient indicates that inlet model B (annular bypass inlet) had the highest external drag. This would be expected from the data of figure 8. The main advantage for this method of bypass is that the inlet always operates supercritically and the possibility of instability due to subcritical operation is avoided. Also most of the bypassed air of models B and C may be utilized in secondary applications (ref. 8) such as for cooling and operating auxiliary equipment. The limitation of the scope of the present investigation precluded variation of inlet geometry and it is believed that a more rigorous design could effectively decrease the net external drag of a bypass inlet that still satisfies the engine

mass-flow requirements through the flight Mach number range. Although the maximum flight Mach number attained for this series of tests was less than 2.0, it is believed that should the maximum Mach numbers required go into the region above 3.0 the relative effectiveness of a bypass inlet compared with similar nonbypass inlets would become more pronounced. This is because the shock losses above a Mach number of 3.0 became prohibitive and the amount of stable subcritical operation of a high Mach number inlet is drastically reduced so that at Mach numbers about 3.0 the use of a bypass would greatly aid inlet and engine matching.

CONCLUDING REMARKS

The results of the present investigation indicate that a fixed-geometry inlet with a fixed bypass of a portion of the inlet air may be used to match typical turbojet-engine air-flow requirements over a wide range of flight speeds, but at a slight cost of external drag. Two models, each with a different type of bypass, closely matched the turbojet-engine air-flow requirements over the test flight Mach number range from 0.8 to 1.95. However, the inlet with the 360° annular bypass, had the highest external drag cofficient as compared with the conical inlet without bypass, and the inlet with the slotted bypass had only slightly higher external drag than the inlet without a bypass. The conical inlet without the bypass (designed to match the engine requirements at a Mach number of 1.0) had slightly less external drag than the slotted bypass model, even after the spillage drag was accounted for.

Langley Aeronautical Laboratory,
National Advisory Committee for Aeronautics,
Langley Field, Va., Oct. 22, 1957.

APPENDIX

PREFLIGHT-DATA REDUCTION AND INTERNAL-DRAG DATA

The mass-flow ratios were calculated using one-dimensional flow relationships as follows:

Mass-flow ratio entering inlet:

$$\left(\frac{w}{w_\infty}\right)_i = \left(\frac{w}{w_\infty}\right)_N + \left(\frac{w}{w_\infty}\right)_{B'} \tag{1}$$

Engine air mass-flow ratio:

$$\left(\frac{w}{w_\infty}\right)_N = \frac{p_N M_N \left(1 + 0.2M_N^2\right)^{1/2} A_N}{p_\infty M_\infty \left(1 + 0.2M_\infty^2\right)^{1/2} A_i} \tag{2}$$

Mass-flow ratio entering bypass:

$$\left(\frac{w}{w_\infty}\right)_{B'} = \frac{p_{B'} M_{B'} \left(1 + 0.2M_{B'}^2\right)^{1/2} A_{B'}}{p_\infty M_\infty \left(1 + 0.2M_\infty^2\right)^{1/2} A_i} \tag{3}$$

Mass-flow ratio entering bypass annular sectors:

$$\left(\frac{w}{w_\infty}\right)_X = \frac{p_X M_X \left(1 + 0.2M_X^2\right)^{1/2} A_X}{p_\infty M_\infty \left(1 + 0.2M_\infty^2\right)^{1/2} A_i} \tag{4}$$

Mass-flow ratio out of slots:

$$\left(\frac{w}{w_\infty}\right)_s = \left(\frac{w}{w_\infty}\right)_{B'} - \left(\frac{w}{w_\infty}\right)_X \tag{5}$$

Internal drag was then computed for engine air mass flow from momentum loss as follows:

$$D_i = \gamma p_\infty M_\infty^2 \left(\frac{w}{w_\infty}\right)_N A_i - \gamma p_N M_N^2 A_N - A_N\left(p_N - p_\infty\right) \tag{6}$$

DECLASSIFIED

Therefore,

$$C_{D,i} = 2\left(\frac{w}{w_\infty}\right)_N \frac{A_i}{A_f} - \frac{2p_N M_N{}^2 A_N}{p_\infty M_\infty{}^2 A_f} - \frac{2A_N}{\gamma M_\infty{}^2 A_f}\left(\frac{p_N}{p_\infty} - 1\right) \tag{7}$$

REFERENCES

1. Allen, J. L., and Beke, Andrew: Force and Pressure Recovery Characteristics at Supersonic Speeds of a Conical Spike Inlet With Bypasses Discharging in an Axial Direction. NACA RM E52K14, 1953.

2. Beke, Andrew, and Allen, J. L.: Force and Pressure-Recovery Characteristics at Supersonic Speeds of a Conical Nose Inlet With Bypasses Discharging Outward From the Body Axis. NACA RM E52L18a, 1953.

3. Allen, J. L., and Beke, Andrew: Force and Pressure Recovery Characteristics at Supersonic Speeds of a Conical Spike Inlet With a Bypass Discharging From the Top or Bottom of the Diffuser in an Axial Direction. NACA RM E53A29, 1953.

4. Wood, Charles C., and Henry, John R.: Bypass-Duct Design for Use With Supersonic Inlets. NACA RM L55L13a, 1956.

5. Allen, J. L., and Beke, Andrew: Performance Comparison at Supersonic Speeds of Inlets Spilling Excess Flow by Means of Bow Shock, Conical Shock, or Bypass. NACA RM E53H11, 1953.

6. Faget, Maxime A., Watson, Raymond S., and Bartlett, Walter A., Jr.: Free-Jet Tests of a 6.5-Inch-Diameter Ram-Jet Engine at Mach Numbers of 1.81 and 2.00. NACA RM L50L06, 1951.

7. Merlet, Charles F., and Putland, Leonard W.: Flight Determination of the Drag of Conical-Shock Nose Inlets With Various Cowling Shapes and Axial Positions of the Center Body at Mach Numbers From 0.8 to 2.0. NACA RM L54G21a, 1954.

8. Hearth, Donald P.: Use of Main-Inlet Bypass to Supply Ejector Exhaust Nozzle at Supersonic Speeds. NACA RM E56K08, 1957.

CONFIDENTIAL

TABLE I.- AREA DISTRIBUTION

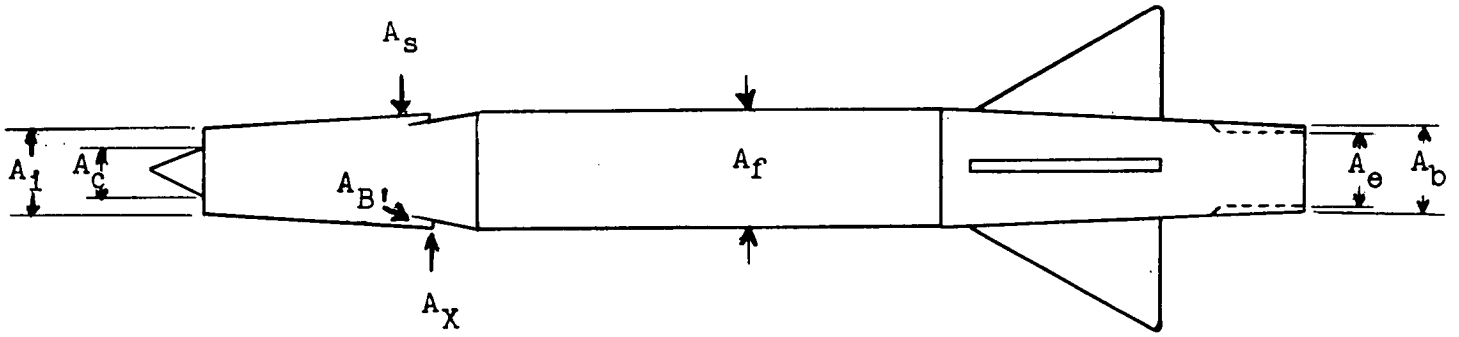

	Models		
	A	B	C
A_i, sq in.	16.909	32.271	18.399
A_f, sq in.	38.485	38.485	38.485
A_e, sq in.	13.364	13.364	13.364
A_i/A_f	0.439	0.839	0.478
A_e/A_i	0.790	0.414	0.726
$A_{B'}$, sq in.	------	------	2.322
A_X, sq in.	------	12.159	1.385
$4A_s$, sq in.	------	------	2.360
A_c, sq in.	4.374	8.296	4.753
$A_i - A_c$, sq in.	12.535	23.975	13.646

CONFIDENTIAL

TABLE II.- TEST POSITIONS

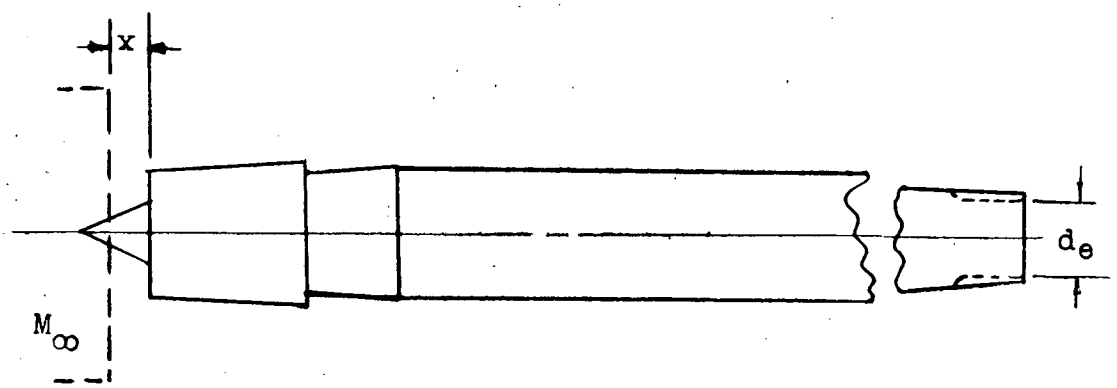

(a) Model B

Test	d_e, in.	x, in.	M_∞
1	3.450	1.0	2.03
2	3.688	1.0	2.03
3	3.912	1.0	2.03
4	4.125	1.0	2.03
5	2.917	1.5	1.62
6	3.450	1.5	1.62
7	3.688	1.5	1.62
8	3.912	1.5	1.62
9	4.125	1.5	1.62
10	2.917	2.5	1.39
11	3.450	2.5	1.39
12	3.688	2.5	1.39
13	3.912	2.5	1.39
14	4.125	2.5	1.39
15	2.917	3.5	1.17
16	3.450	3.5	1.17
17	3.688	3.5	1.17
18	3.912	3.5	1.17
19	4.125	3.5	1.17

(b) Model C

Test	d_e, in.	x, in.	M_∞
20	3.450	1.75	2.03
21	3.688	1.75	2.03
22	4.125	1.75	2.03
23	3.450	1.25	1.62
24	3.688	1.25	1.62
25	4.125	1.25	1.62
26	3.450	2.0	1.39
27	3.688	2.0	1.39
28	4.125	2.0	1.39
29	3.450	2.75	1.17
30	3.688	2.75	1.17
31	4.125	2.75	1.17
32	3.450	2.75	1.06
33	3.450	2.75	.92
34	3.450	2.75	.81
35	3.688	2.75	1.04
36	3.688	2.75	.99
37	3.688	2.75	.90
38	4.125	2.75	1.08
39	4.125	2.75	.96
40	4.125	2.75	.89

DECLASSIFIED

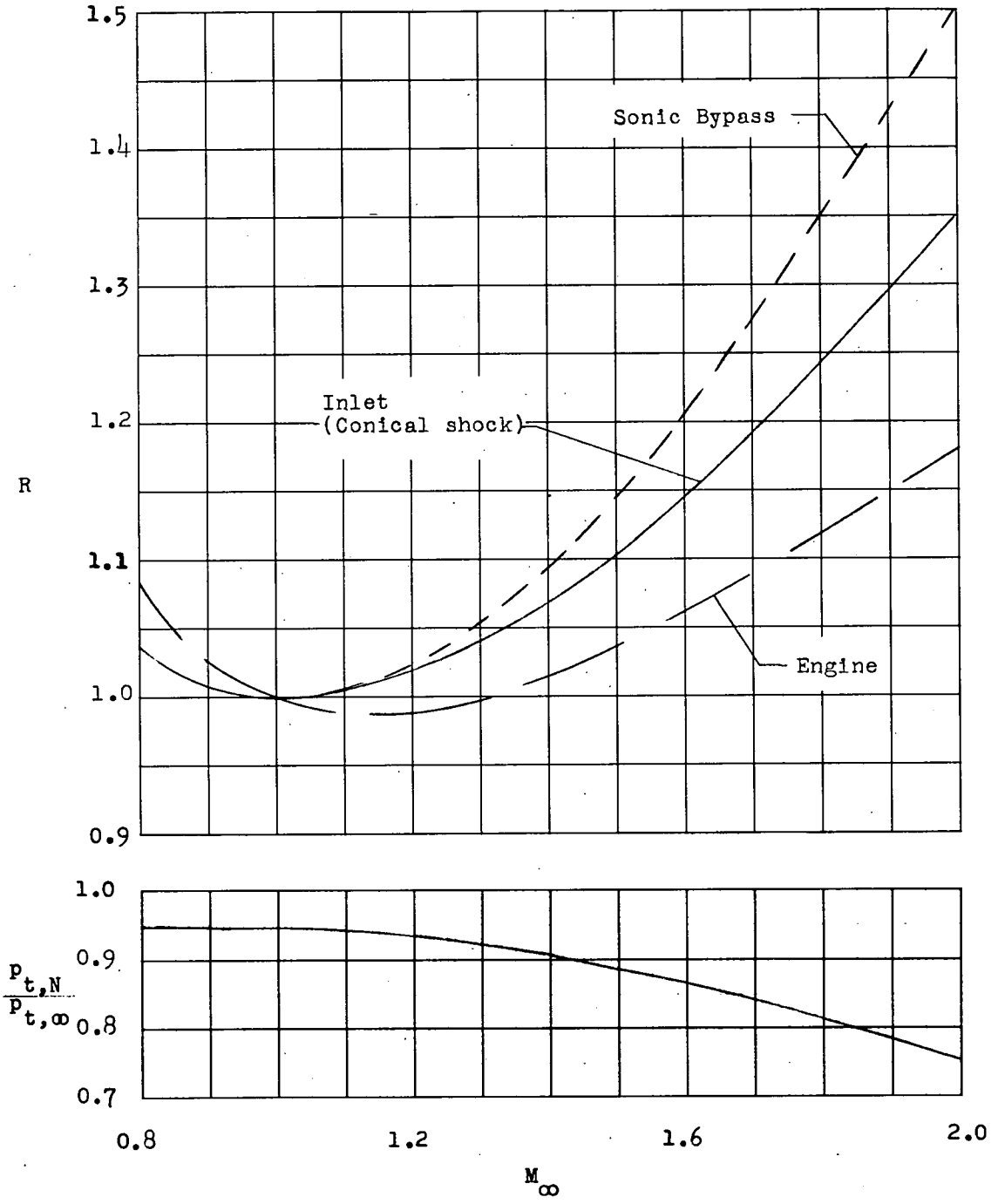

Figure 1.- Typical regulation curves, matched at $M_\infty = 1.0$.

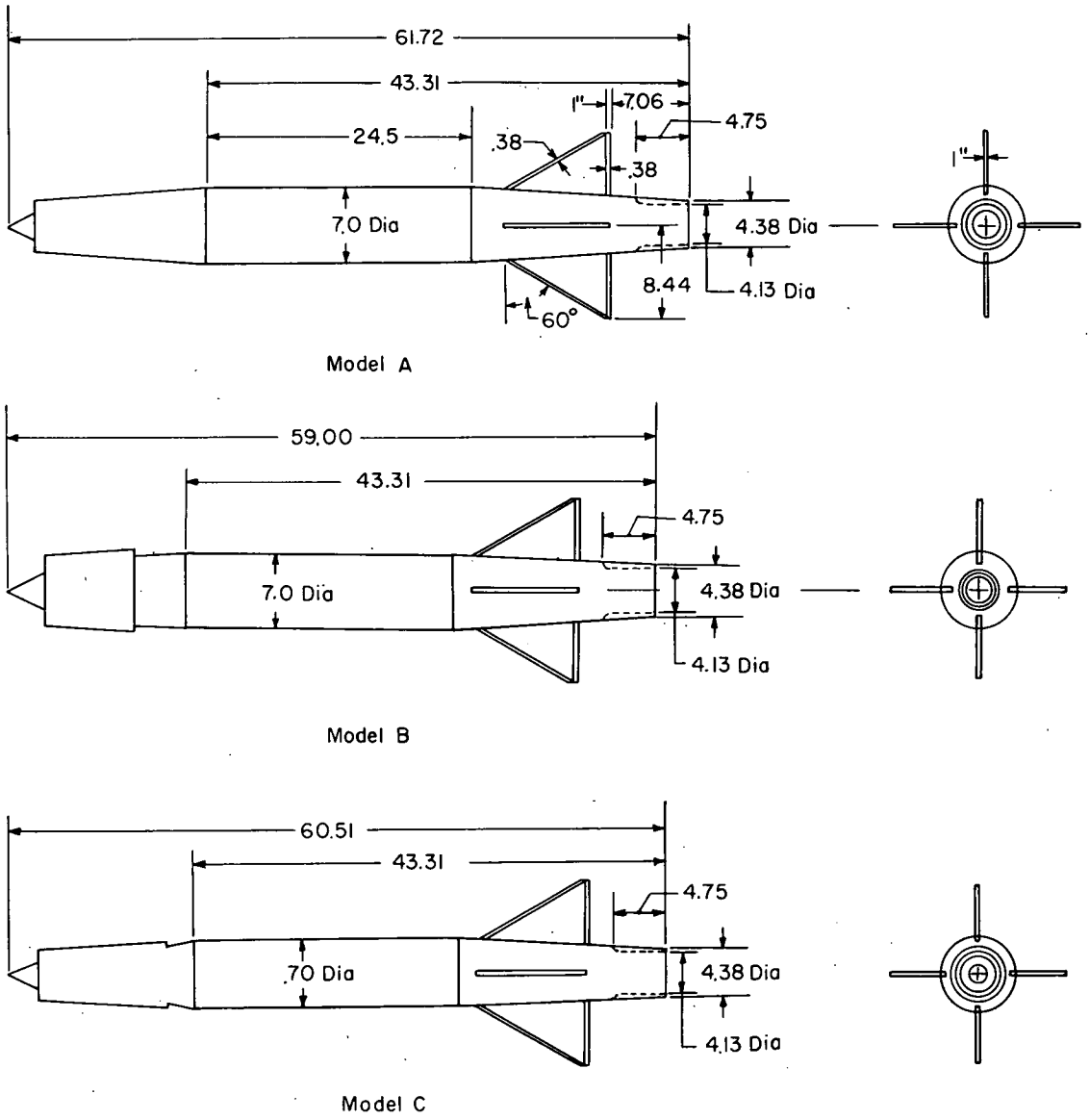

(a) Sketches.

Figure 2.- Sketches and photographs of the models showing the three configurations. All dimensions are in inches.

DECLASSIFIED

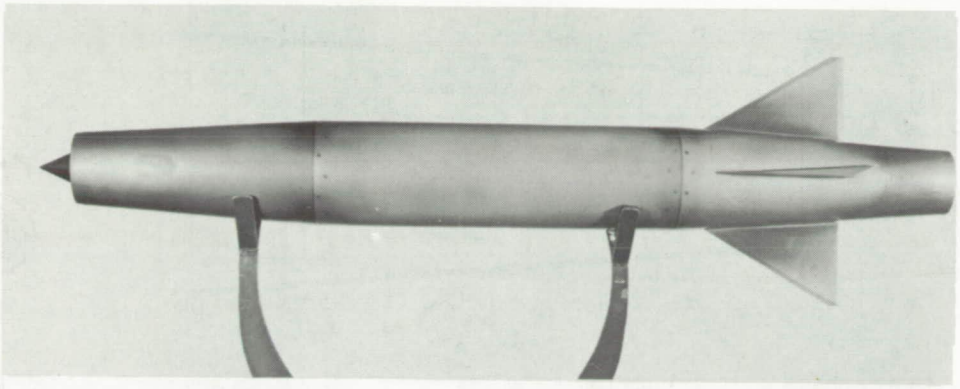

Model A L-86790

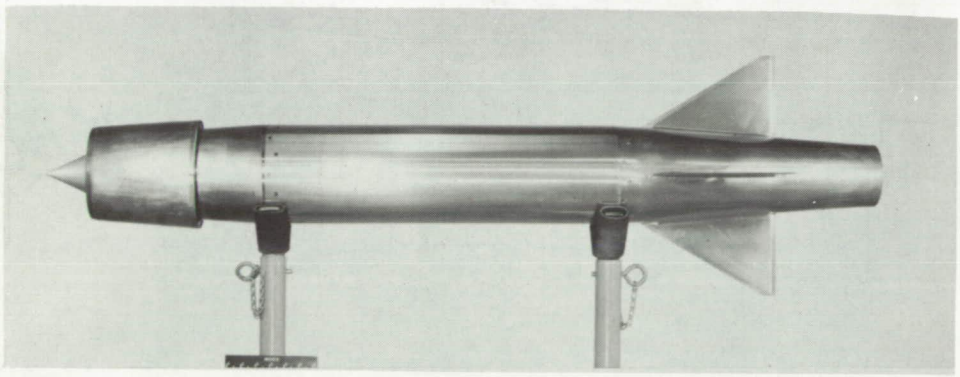

Model B L-88927

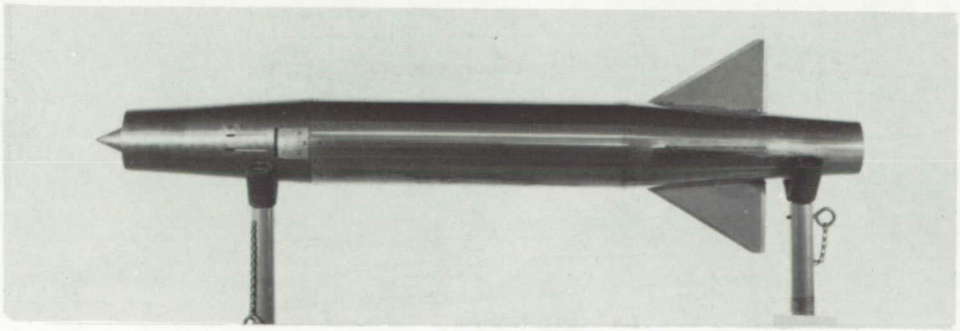

Model C

(b) Photographs of models. L-96554

Figure 2.- Concluded.

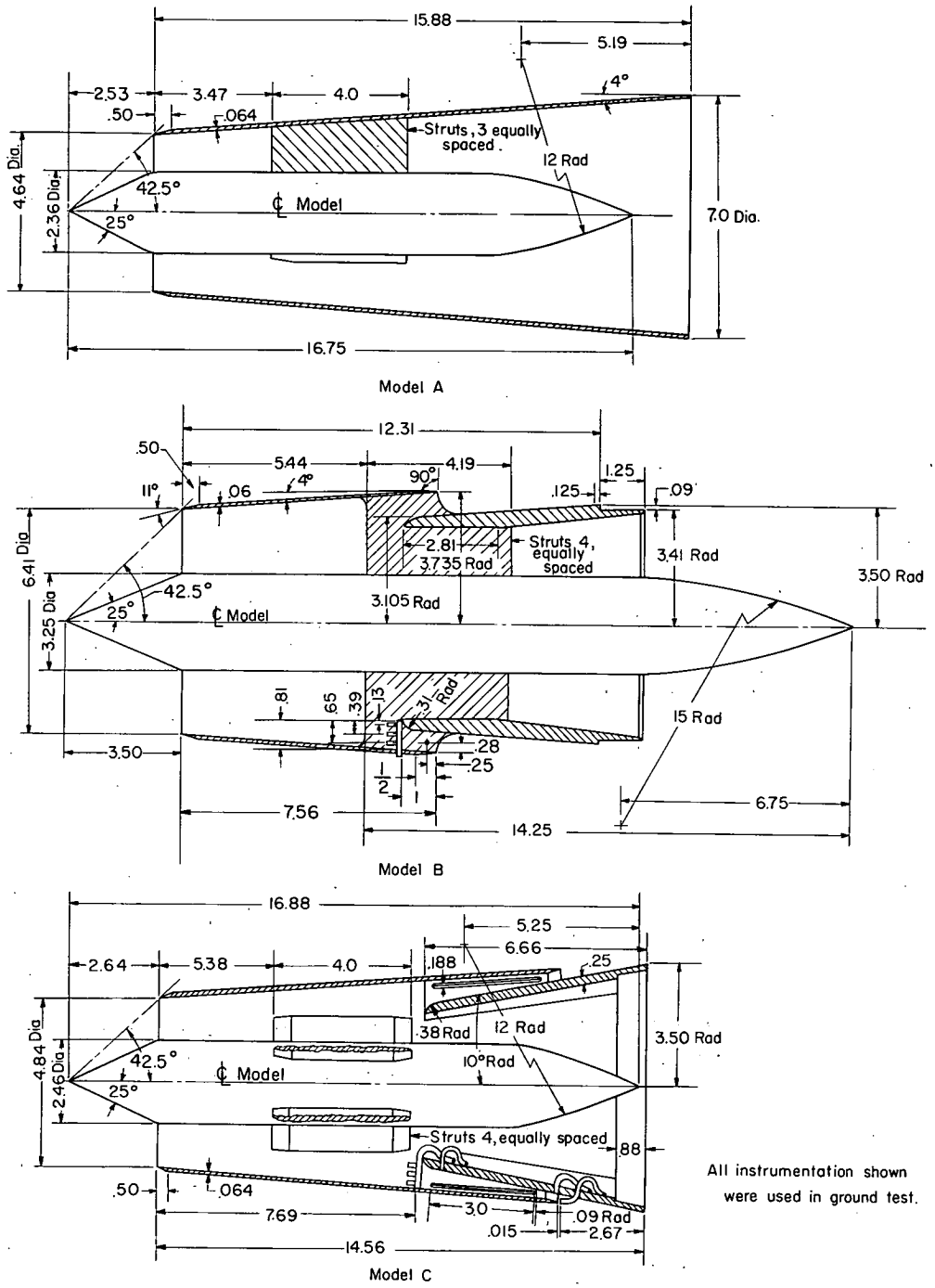

(a) Sketches.

Figure 3.- Details of cowling shapes. All dimensions are in inches.

DECLASSIFIED

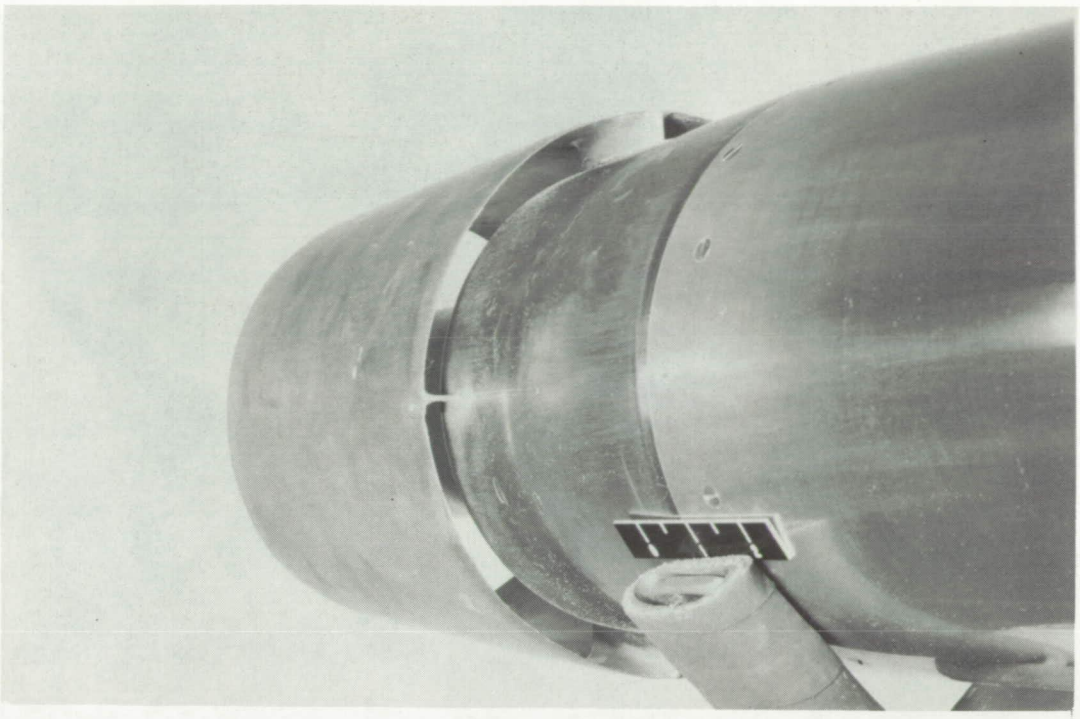

Model B L-88926

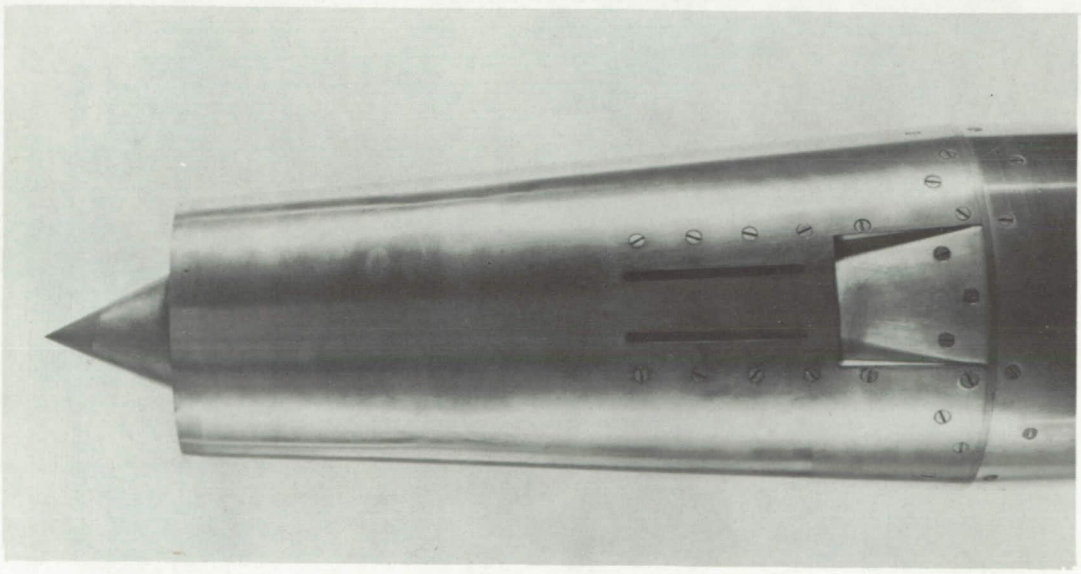

Model C

(b) Photographs of cowlings. L-96555

Figure 3.- Concluded.

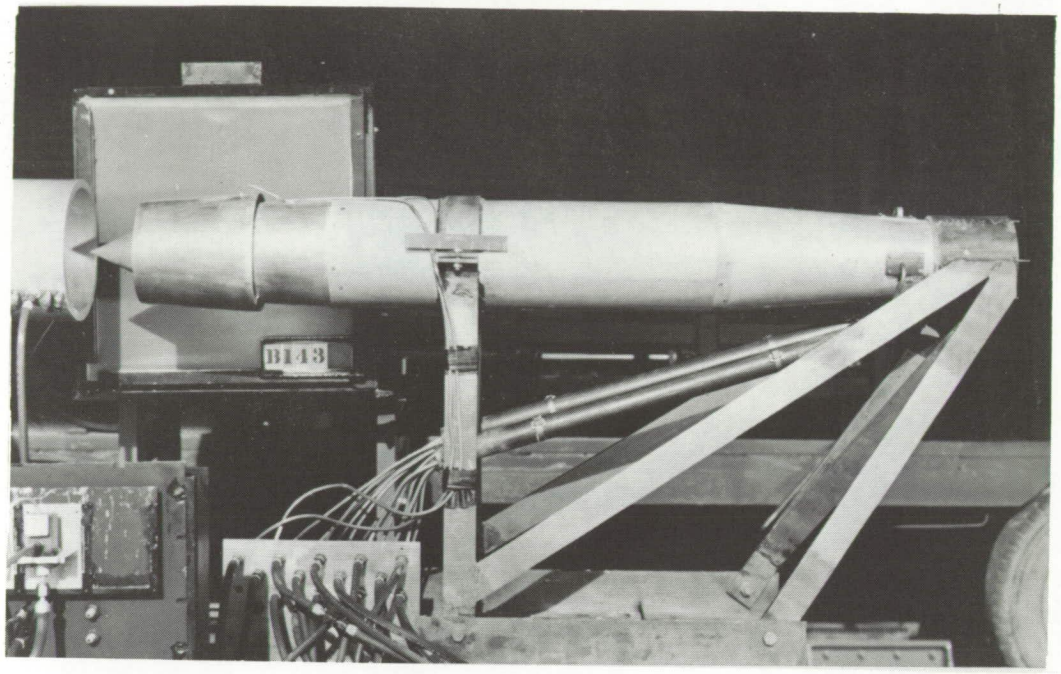

Model B L-88351

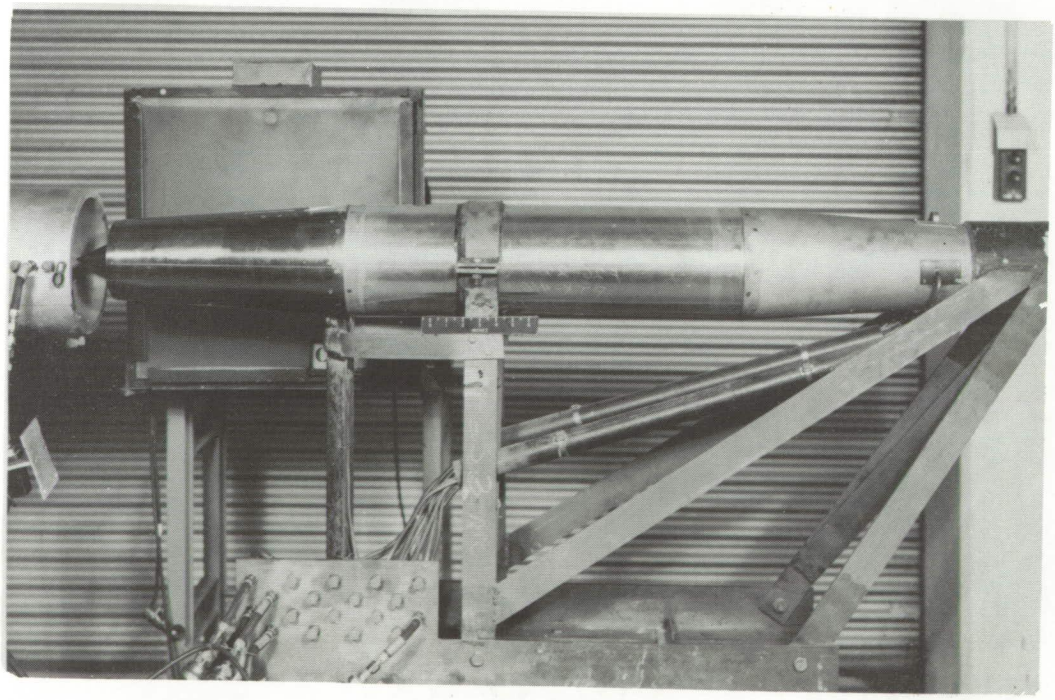

Model C

L-96093

Figure 4.- Photographs of models mounted on test stand in preflight jet.

DECLASSIFIED

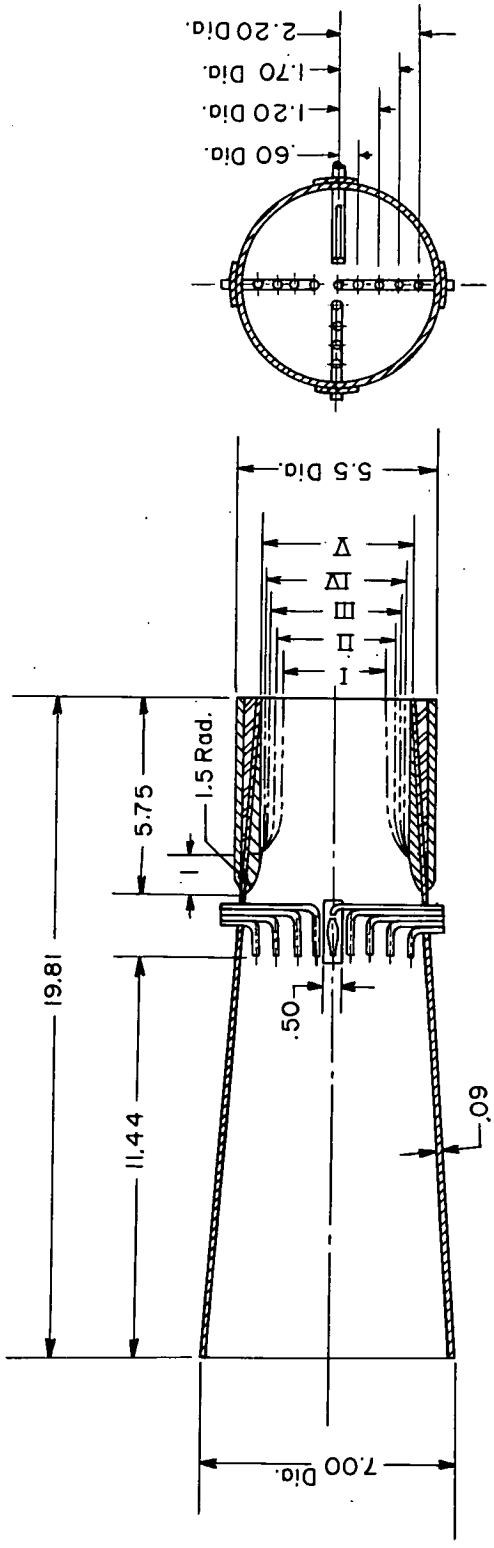

Figure 5.- Sketch showing ground-test tail cone with five exits. All dimensions are in inches.

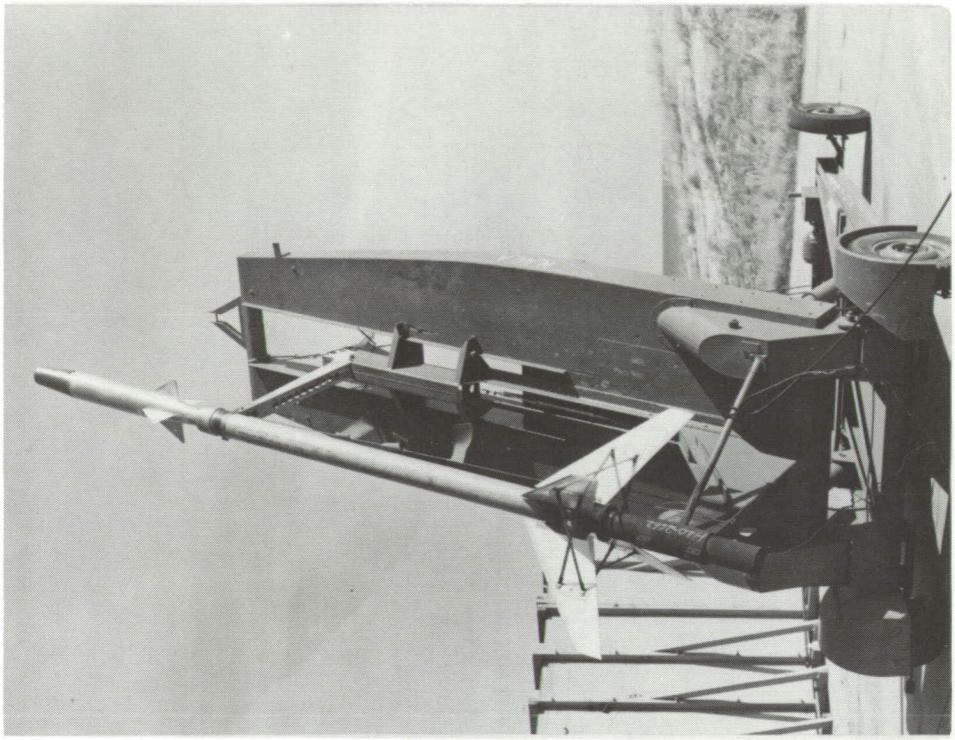

Model C L-96735

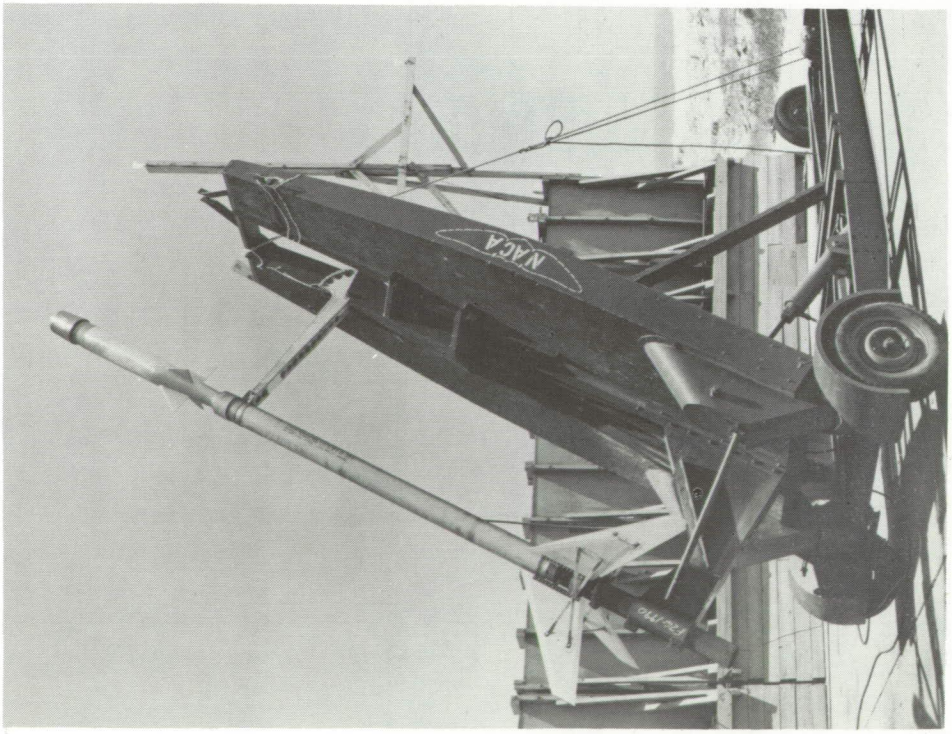

Model B L-89526

Figure 6.- Photographs of models and booster on launcher.

DECLASSIFIED

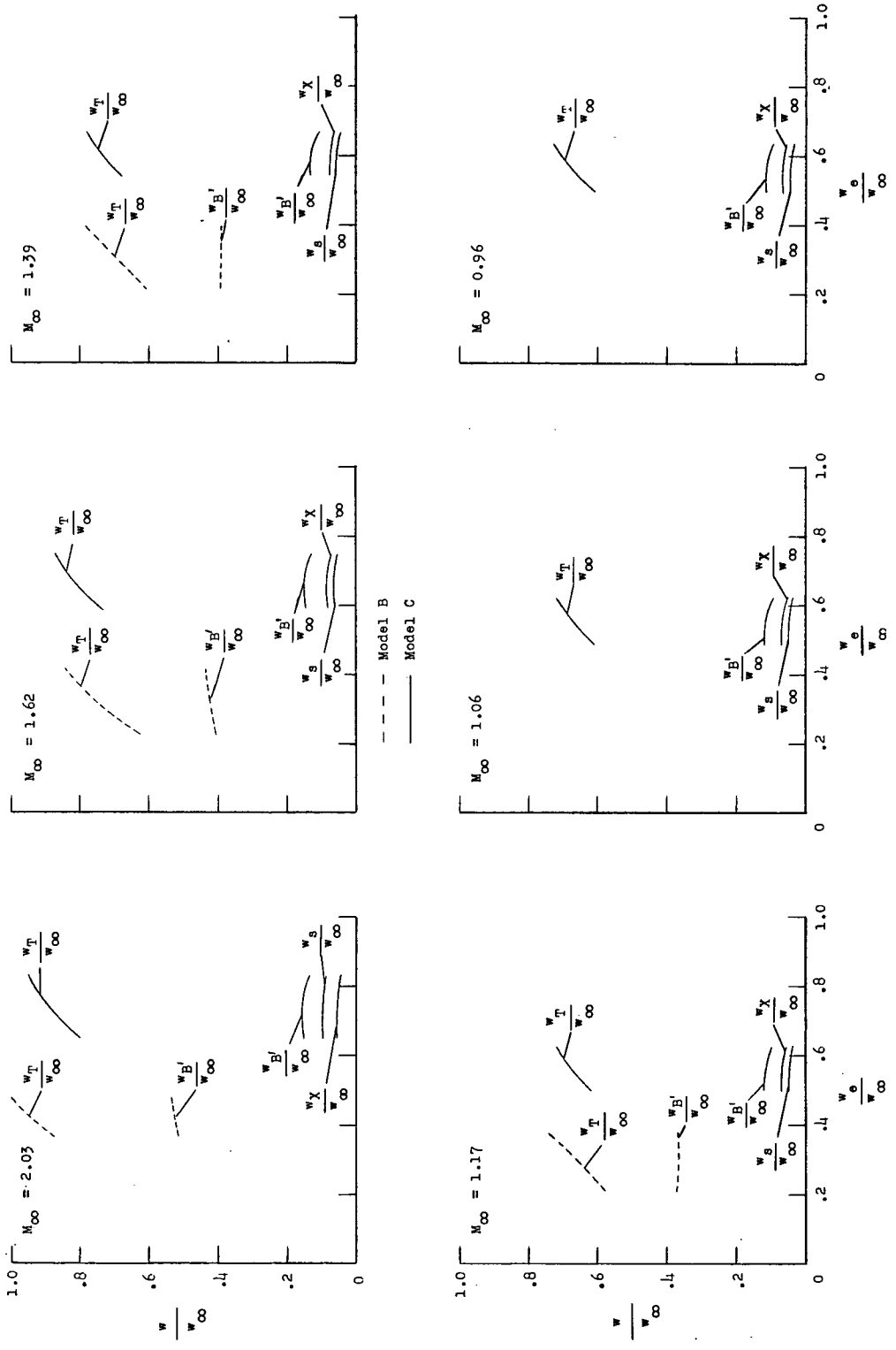

Figure 7.- Variation of mass-flow ratio through the engine, bypass, and slots for each free-stream Mach number ground tested.

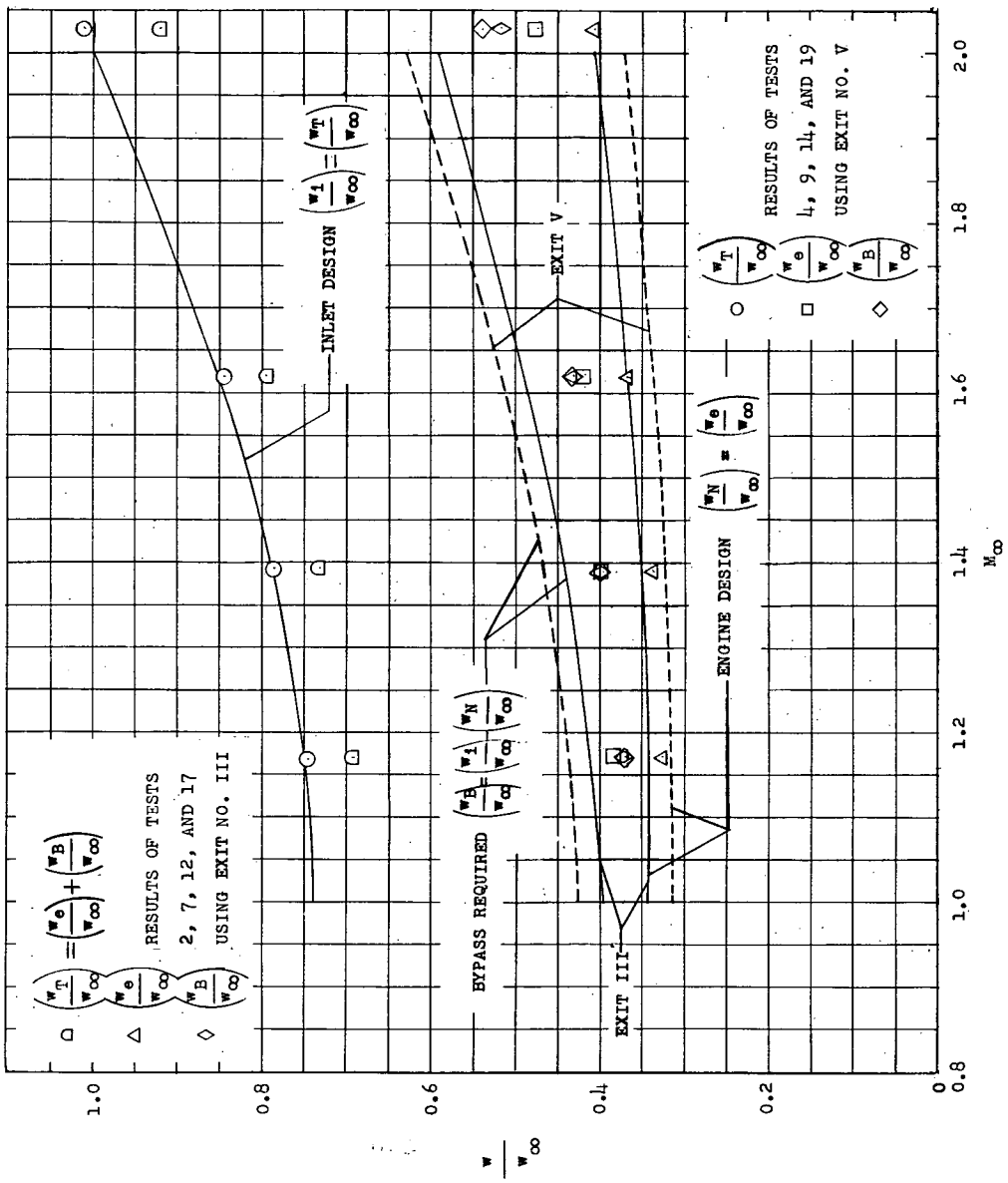

(a) Model B.

Figure 8.- Variation of air mass-flow ratio with free-stream Mach number for models B and C.

DECLASSIFIED

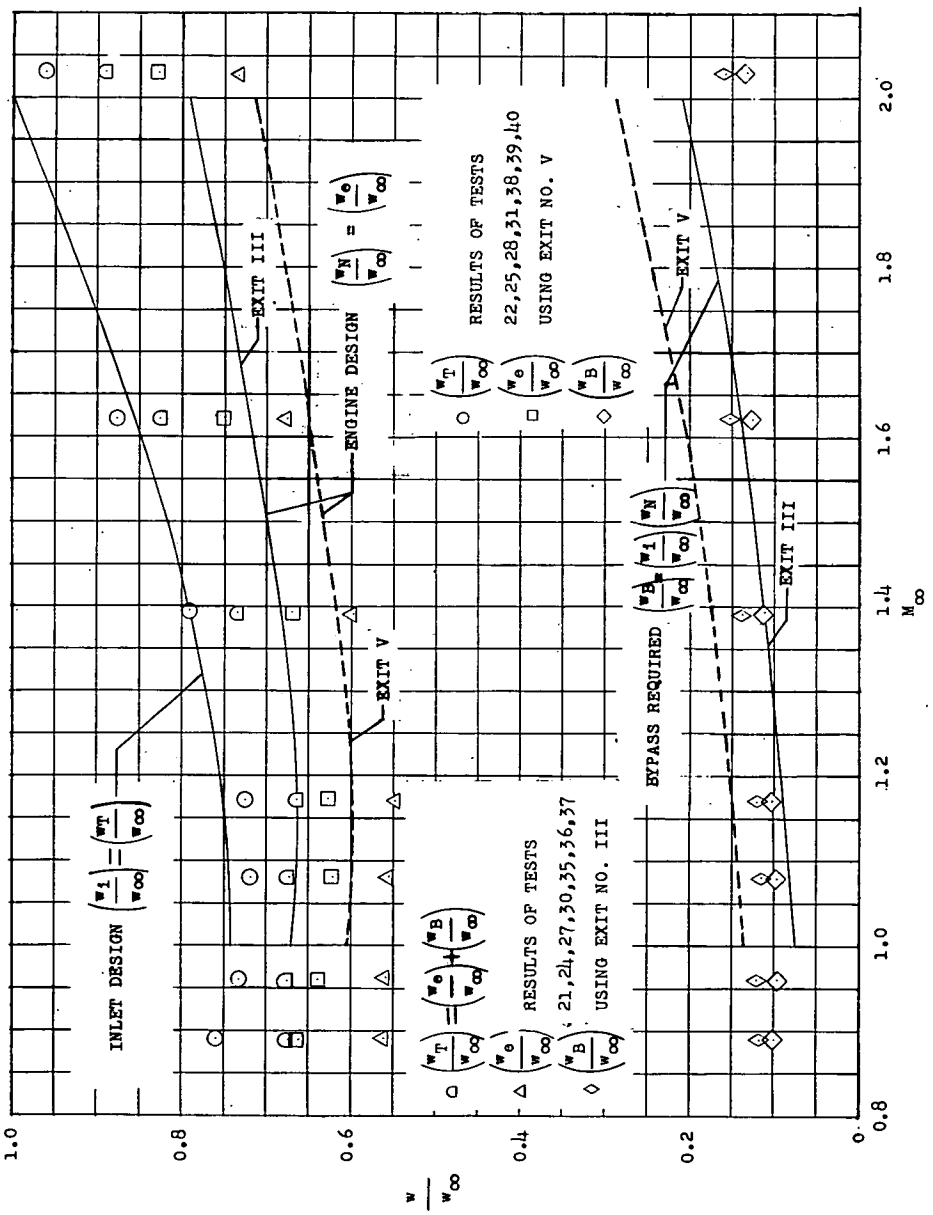

(b) Model C.

Figure 8.- Concluded.

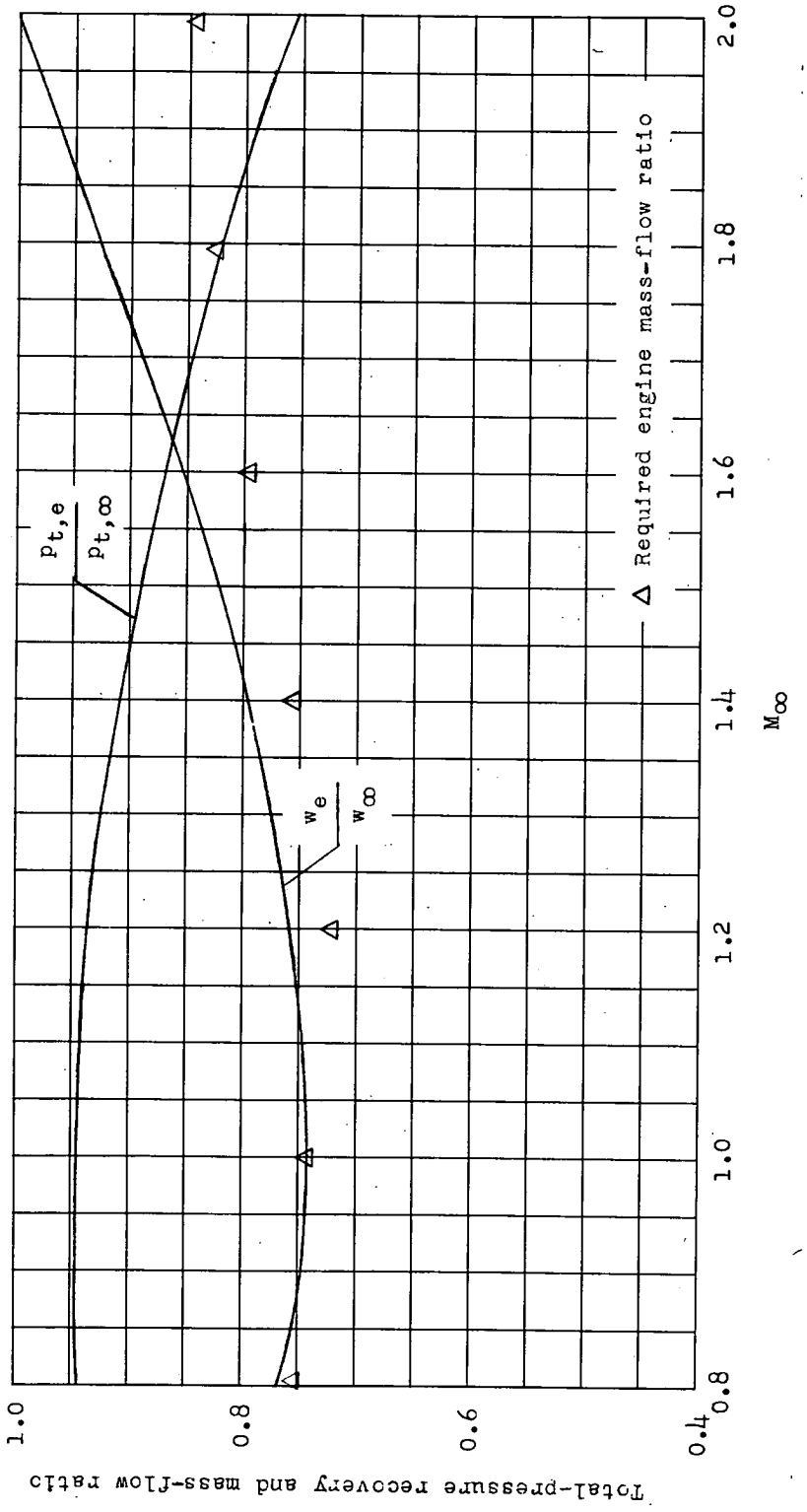

Figure 9.- Variation of calculated total-pressure recovery and engine mass-flow ratio with free-stream Mach numbers for model A with a supercritical inlet.

DECLASSIFIED

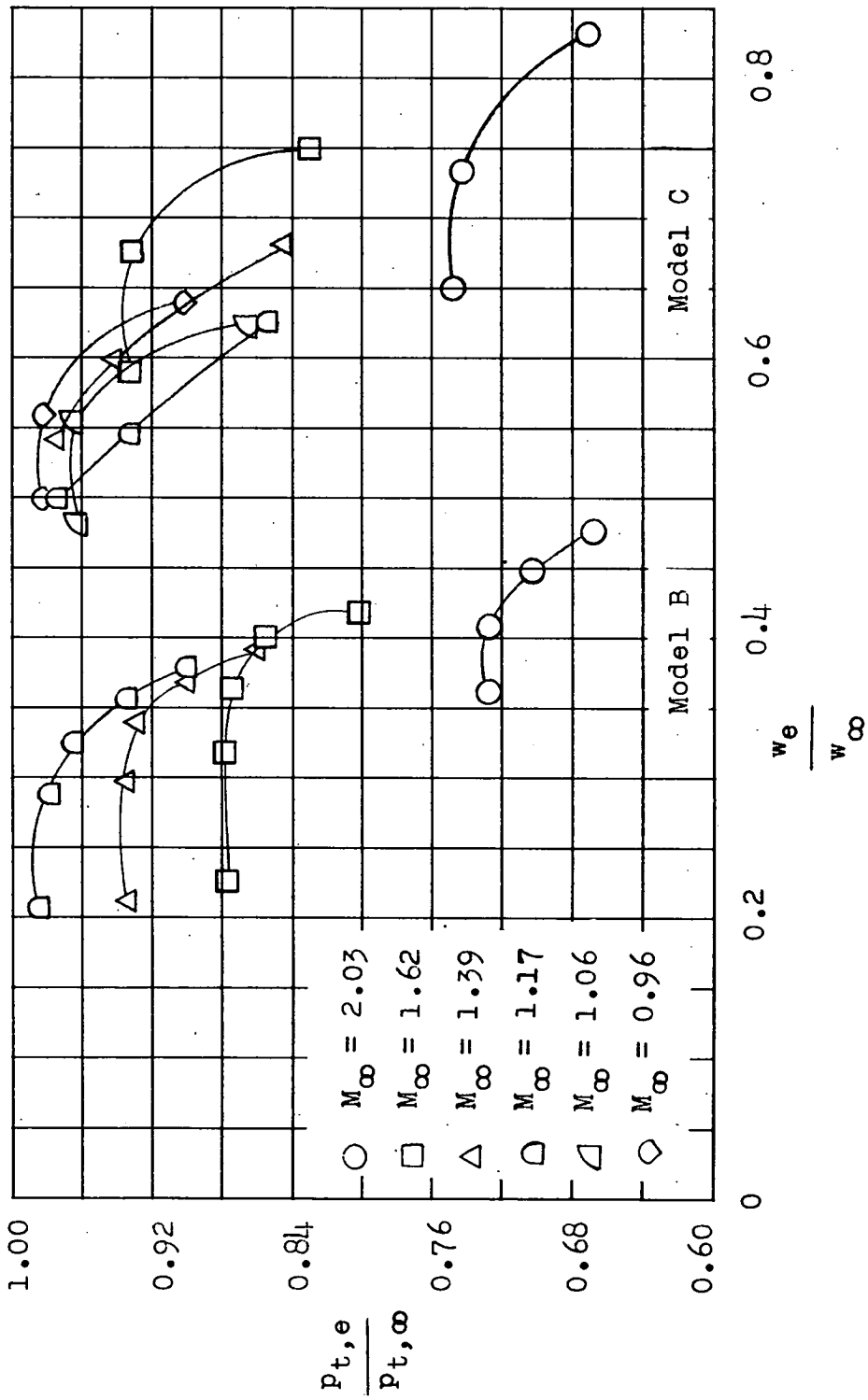

Figure 10.- Variation of total-pressure recovery with exit mass-flow ratio from ground tests for models B and C.

CONFIDENTIAL

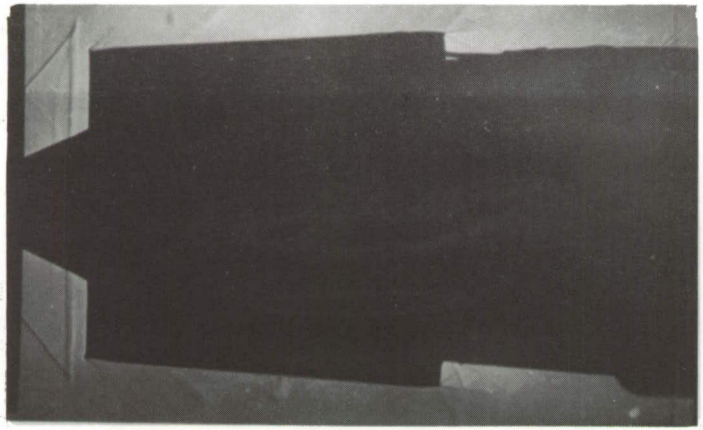

(a) Model B; $M_\infty = 1.62$.

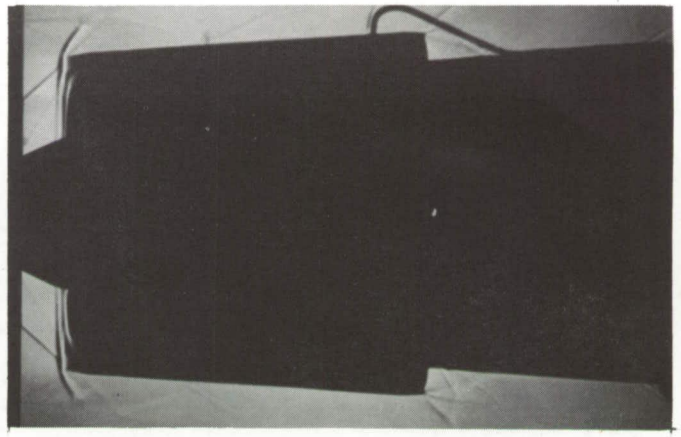

(b) Model B; $M_\infty = 2.03$.

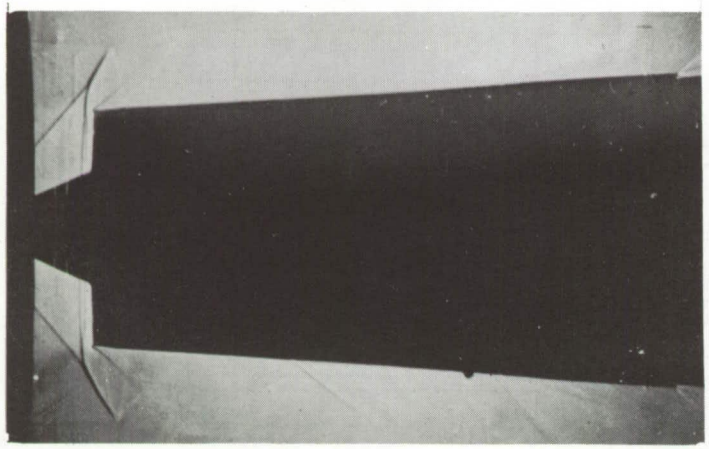

(c) Model C; $M_\infty = 1.62$.

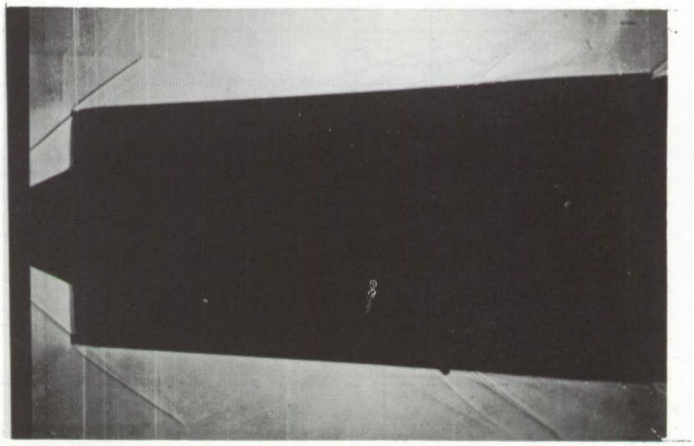

(d) Model C; $M_\infty = 2.03$.

L-57-4406

Figure 11.- Shadowgraph pictures of models B and C with exit V in preflight tunnel.

CONFIDENTIAL

DECLASSIFIED

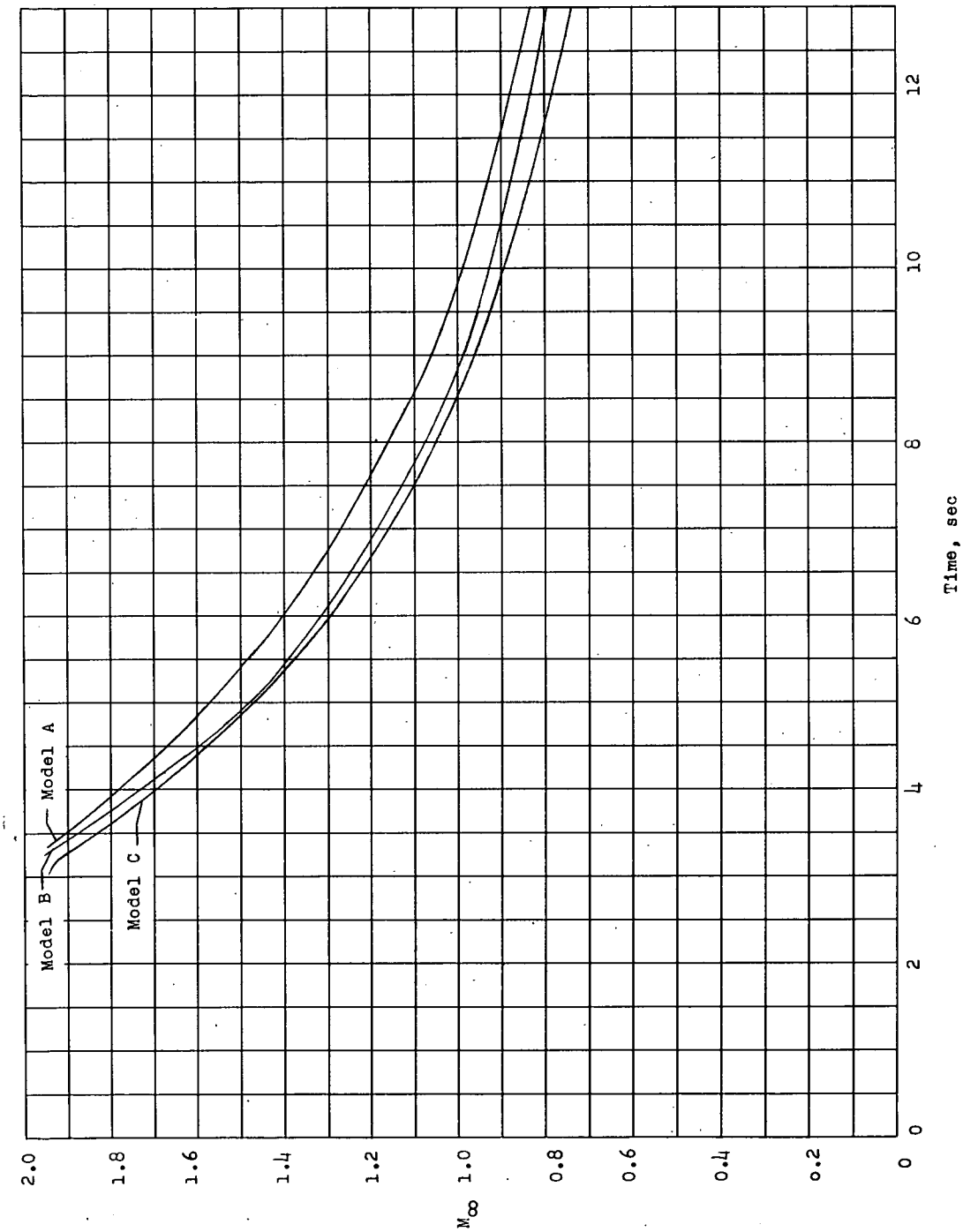

Figure 12.- Variation of free-stream Mach number with time for the three models flight tested.

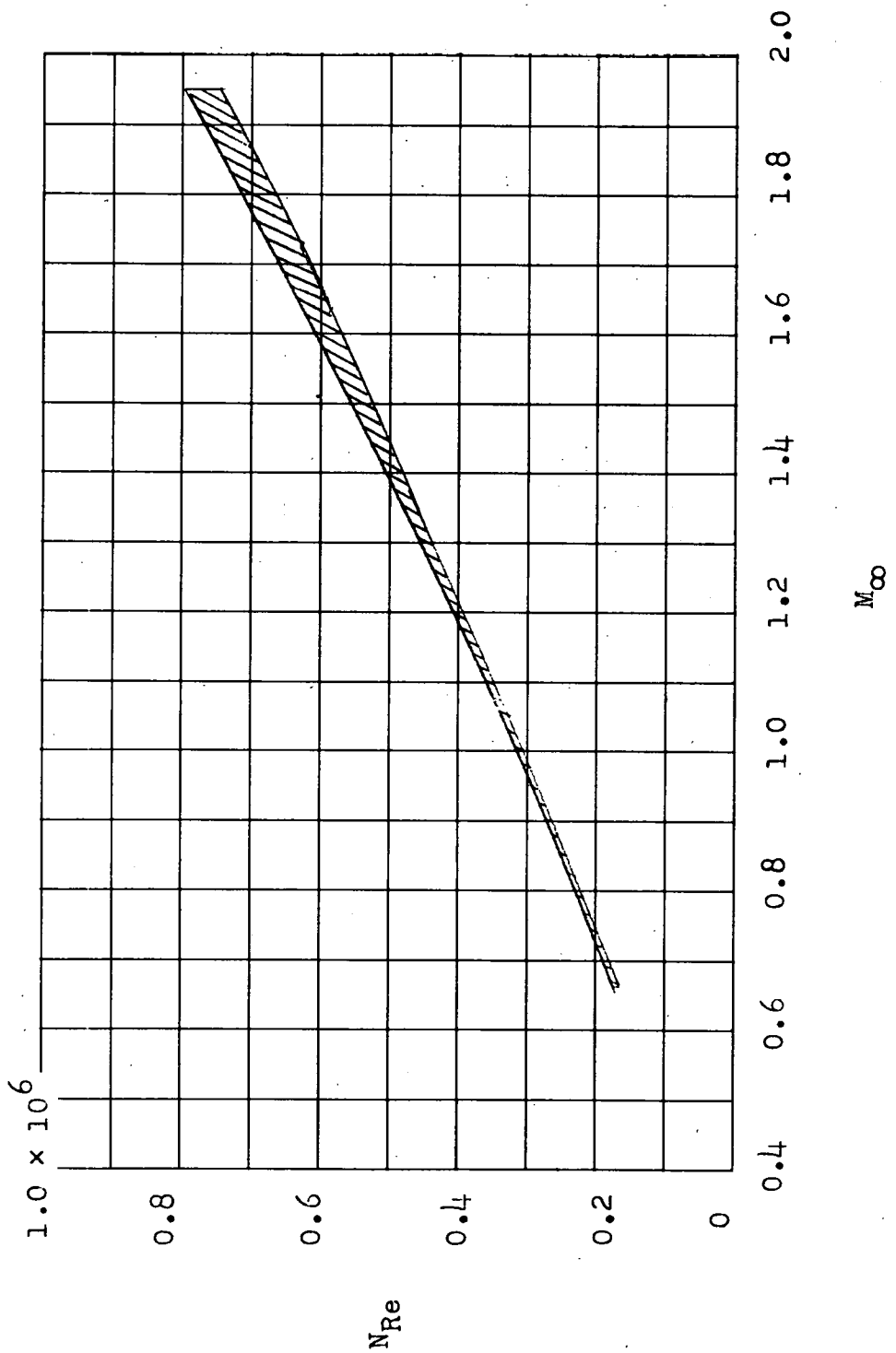

Figure 13.- Variation of Reynolds number with free-stream Mach number.

DECLASSIFIED

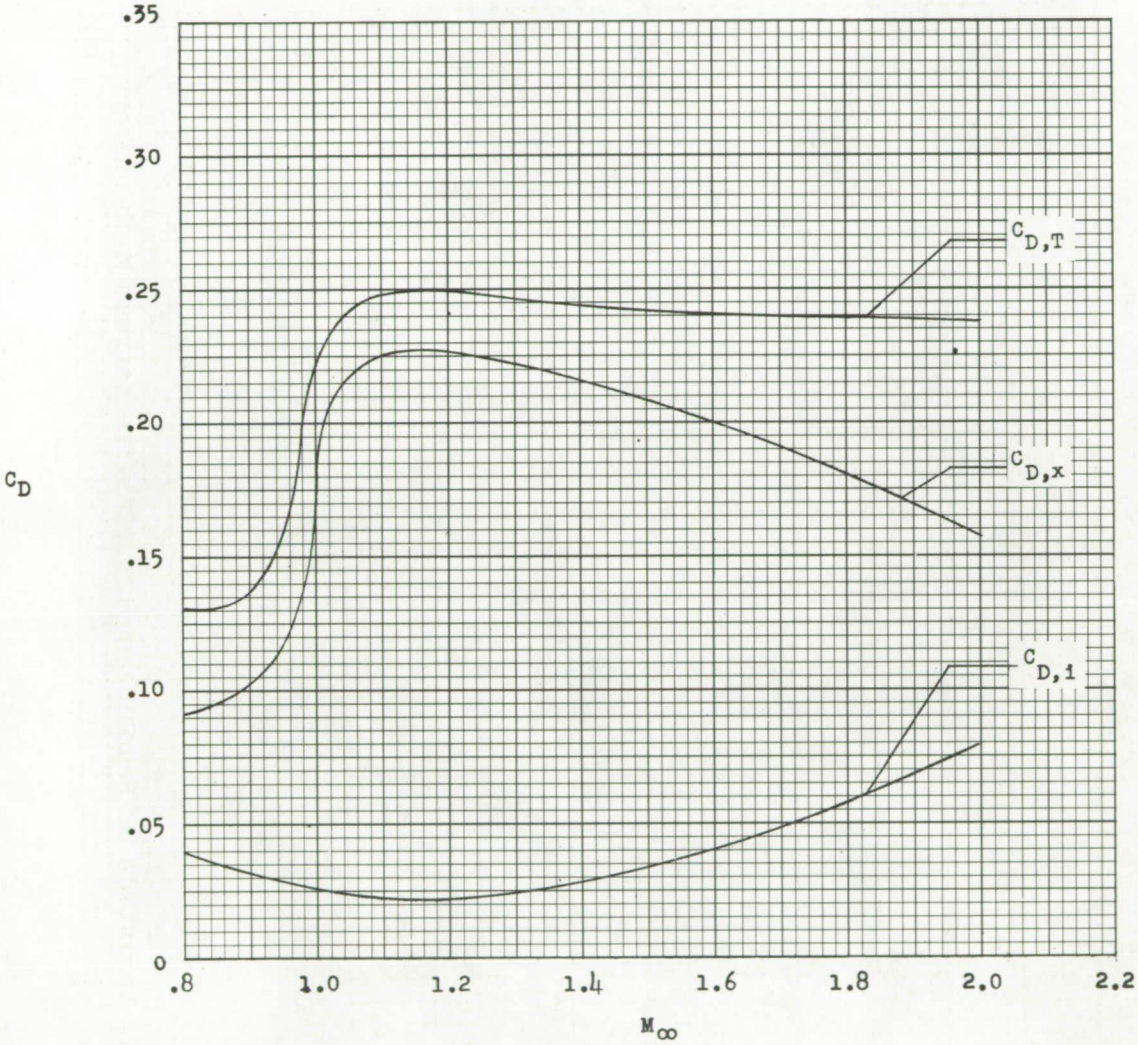

(a) Model A.

Figure 14.- Variation of total drag, external drag, and internal drag with free-stream Mach number for the three flight models.

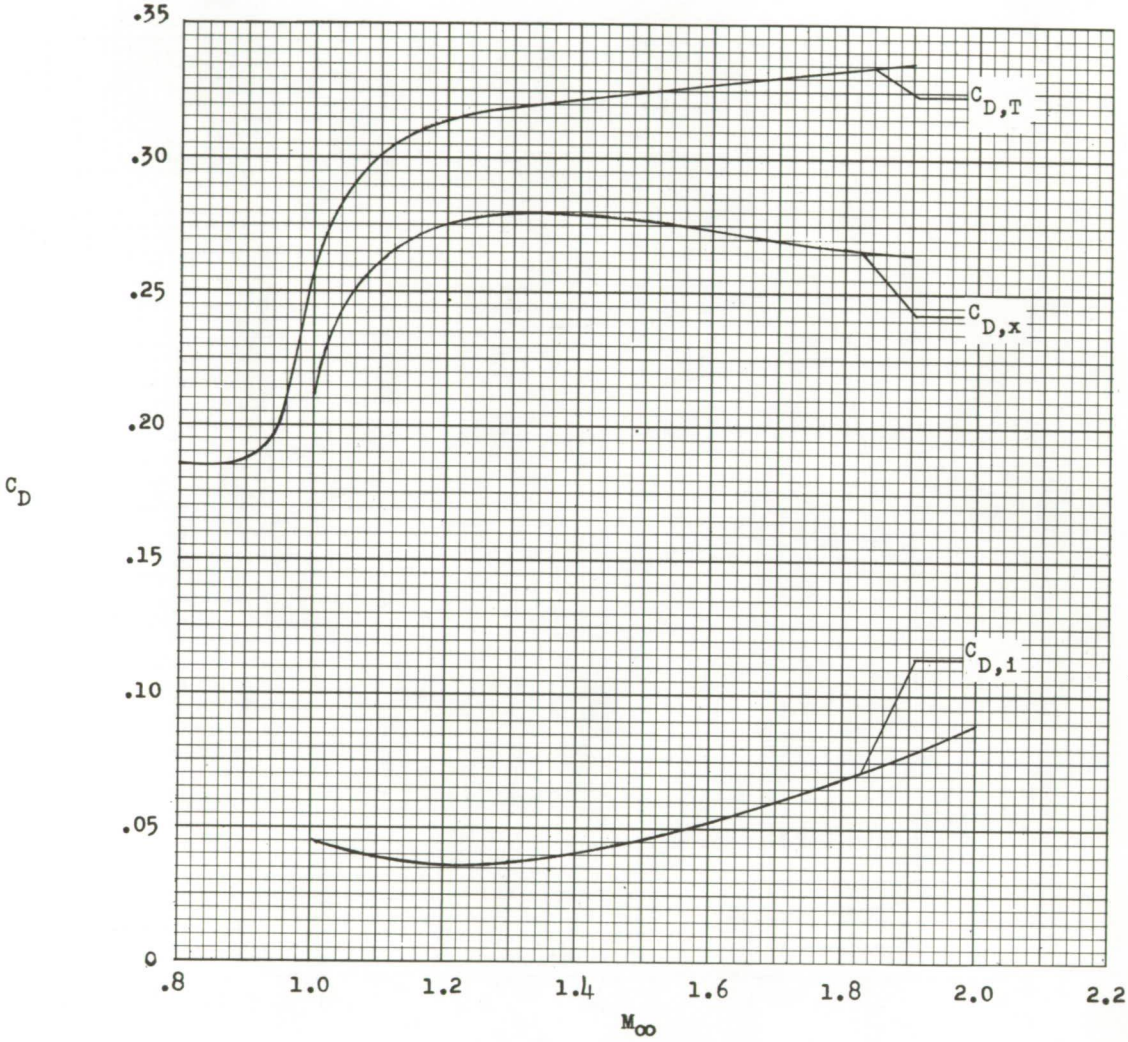

(b) Model B.

Figure 14.- Continued.

DECLASSIFIED

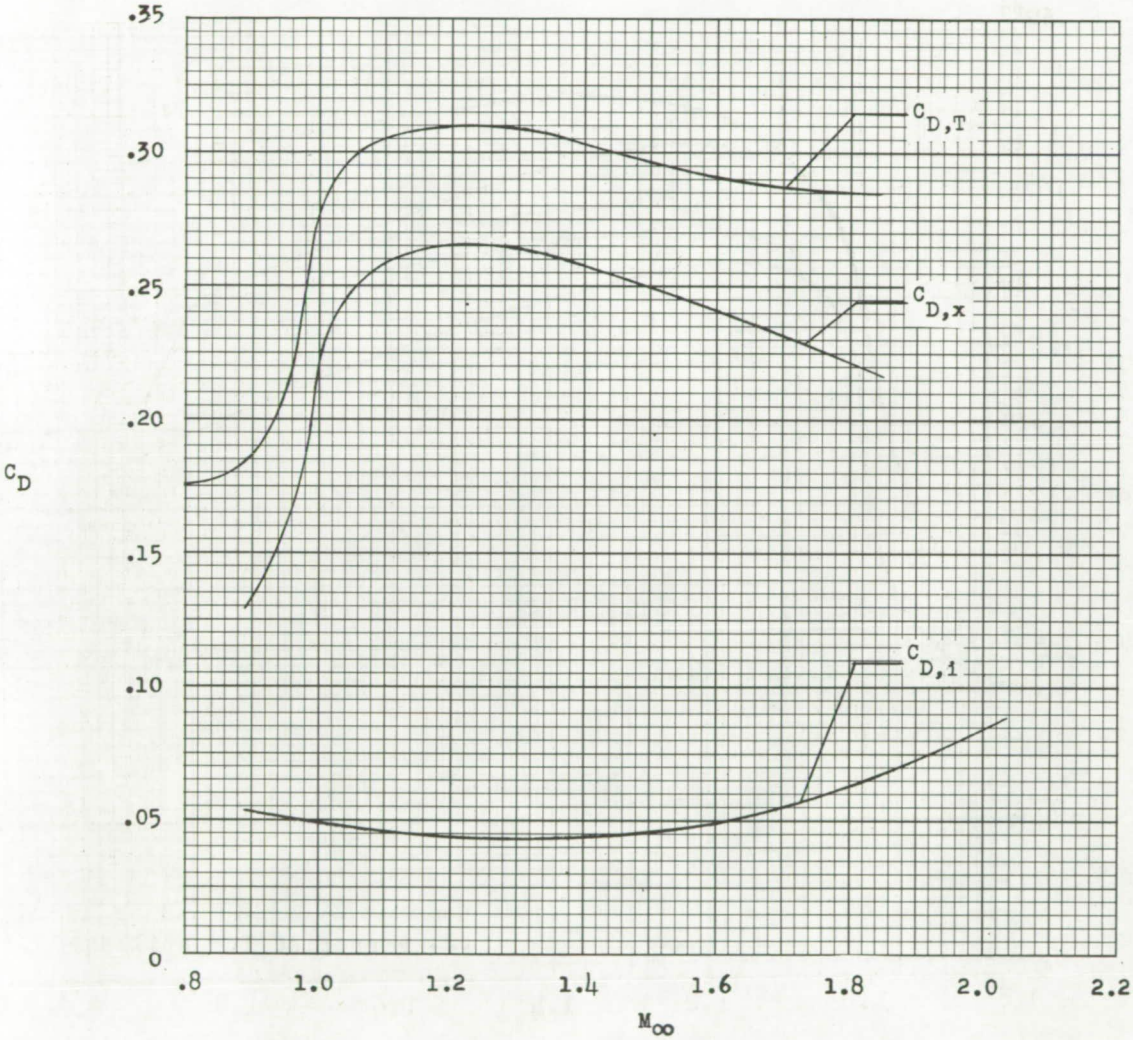

(c) Model C.

Figure 14.- Concluded.

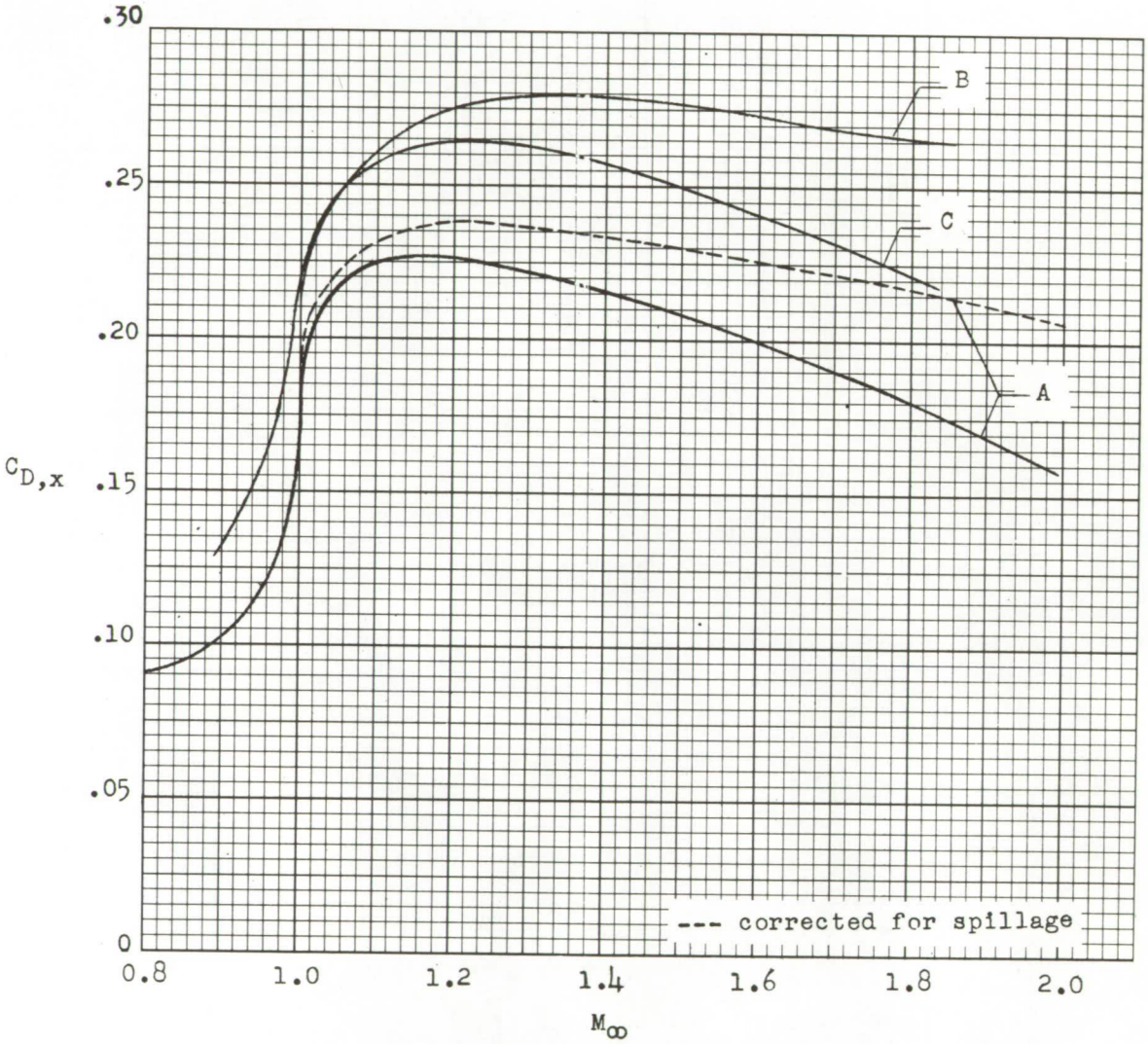

Figure 15.- Comparison of external drag coefficients for models A, B, and C.

NACA - Langley Field, Va.

NOTES: (1) Reynolds number is based on the diameter of a circle with the same area as that of the capture area of the inlet.

(2) The symbol * denotes the occurrence of buzz.

Report and facility	Description			Test parameters				Test data				Performance		Remarks
	Configuration	Number of oblique shocks	Type of boundary-layer control	Free-stream Mach number	Reynolds number $\times 10^{-6}$	Angle of attack, deg	Angle of yaw, deg	Drag	Inlet-flow profile	Discharge-flow profile	Flow picture	Maximum total-pressure recovery	Mass-flow ratio	
CONFID. RM L57K14 Preflight jet and flight tests, PARD	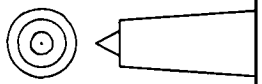	1 Isen-tropic	None	Flight: 0.80 to 2.00	Flight: 1.16 to 5.35	0	0	✓				0.940	0.74 - 1.0	Theoretical
CONFID. RM L57K14 Preflight jet and flight tests, PARD	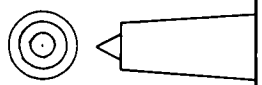	1 Isen-tropic	None	Flight: 0.80 to 2.00	Flight: 1.16 to 5.35	0	0	✓				0.940	0.74 - 1.0	Theoretical
CONFID. RM L57K14 Preflight jet and flight tests, PARD	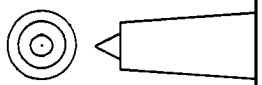	1 Isen-tropic	None	Flight: 0.80 to 2.00	Flight: 1.16 to 5.35	0	0	✓				0.940	0.74 - 1.0	Theoretical
CONFID. RM L57K14 Preflight jet and flight tests, PARD	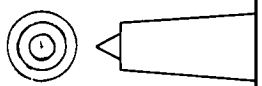	1 Isen-tropic	None	Flight: 0.80 to 2.00	Flight: 1.16 to 5.35	0	0	✓				0.940	0.74 - 1.0	Theoretical

Bibliography

These strips are provided for the convenience of the reader and can be removed from this report to compile a bibliography of NACA inlet reports. This page is being added only to inlet reports and is on a trial basis.

CONFIDENTIAL

CONFIDENTIAL

NOTES: (1) Reynolds number is based on the diameter of a circle with the same area as that of the capture area of the inlet.

(2) The symbol * denotes the occurrence of buzz.

Report and facility	Description			Test parameters				Test data				Performance		Remarks
	Configuration	Number of oblique shocks	Type of boundary-layer control	Free-stream Mach number	Reynolds number $\times 10^{-6}$	Angle of attack, deg	Angle of yaw, deg	Drag	Inlet-flow profile	Discharge-flow profile	Flow picture	Maximum total-pressure recovery	Mass-flow ratio	
CONFID. RM L57K14 Preflight jet and flight tests, PARD	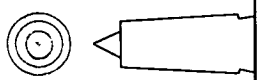	1 Isen-tropic	None	Sea L.: 2.03 1.62 1.39 1.17 1.06 .96 Flight: .80-1.84	Sea level: 5.82 4.64 3.99 3.36 3.04 2.76 Flight: 1.13 - 5.32	0 0 0 0 0 0 0	0 0 0 0 0 0 0	✓				0.749 .936 .974 .976 .966 .984	0.80 - 0.95 .73 - .87 .68 - .78 .62 - .72 .62 - .72 .61 - .73	Shadowgraphs
CONFID. RM L57K14 Preflight jet and flight tests, PARD	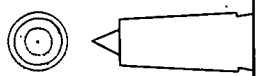	1 Isen-tropic	None	Sea L.: 2.03 1.62 1.39 1.17 1.06 .96 Flight: .80-1.84	Sea level: 5.82 4.64 3.99 3.36 3.04 2.76 Flight: 1.13 - 5.32	0 0 0 0 0 0 0	0 0 0 0 0 0 0	✓				0.749 .936 .974 .976 .966 .984	0.80 - 0.95 .73 - .87 .68 - .78 .62 - .72 .62 - .72 .61 - .73	Shadowgraphs
CONFID. RM L57K14 Preflight jet and flight tests, PARD	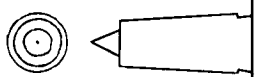	1 Isen-tropic	None	Sea L.: 2.03 1.62 1.39 1.17 1.06 .96 Flight: .80-1.84	Sea level: 5.82 4.64 3.99 3.36 3.04 2.76 Flight: 1.13 - 5.32	0 0 0 0 0 00 0	0 0 0 0 0 0 0	✓				0.749 .936 .974 .976 .966 .984	0.80 - 0.95 .73 - .87 .68 - .78 .62 - .72 .62 - .72 .61 - .73	Shadowgraphs
CONFID. RM L57K14 Preflight jet and flight tests, PARD	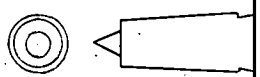	1 Isen-tropic	None	Sea L.: 2.03 1.62 1.39 1.17 1.06 .96 Flight: .80-1.84	Sea level: 5.82 4.64 3.99 3.36 3.04 2.76 Flight: 1.13 - 5.32	0 0 0 0 0 0 0	0 0 0 0 0 0 0	✓				0.749 .936 .974 .976 .966 .984	0.80 - 0.95 .73 - .87 .68 - .78 .62 - .72 .62 - .72 .61 - .73	Shadowgraphs

Bibliography

These strips are provided for the convenience of the reader and can be removed from this report to compile a bibliography of NACA inlet reports. This page is being added only to inlet reports and is on a trial basis.

CONFIDENTIAL

CONFIDENTIAL

NOTES: (1) Reynolds number is based on the diameter of a circle with the same area as that of the capture area of the inlet.

(2) The symbol * denotes the occurrence of buzz.

Report and facility	Description			Test parameters				Test data				Performance		Remarks
	Configuration	Number of oblique shocks	Type of boundary-layer control	Free-stream Mach number	Reynolds number $\times 10^{-6}$	Angle of attack, deg	Angle of yaw, deg	Drag	Inlet-flow profile	Discharge-flow profile	Flow picture	Maximum total-pressure recovery	Mass-flow ratio	
CONFID. RM L57K14 Preflight jet and flight tests, PARD	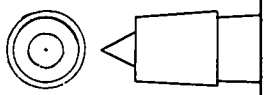	1 Isen-tropic	None	Sea level: 2.03 1.62 1.39 1.17 Flight: 0.80 to 1.90	Sea level: 7.70 6.13 5.27 4.44 Flight: 1.60 to 6.78	0 0 0 0 0	0 0 0 0 0	✓				0.729 .878 .938 .988	0.87 - 1.0 .62 - .85 .61 - .78 .58 - .74	Shadowgraphs
CONFID. RM L57K14 Preflight jet and flight tests, PARD	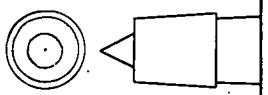	1 Isen-tropic	None	Sea level: 2.03 1.62 1.39 1.17 Flight: 0.80 to 1.90	Sea level: 7.70 6.13 5.27 4.44 Flight: 1.60 to 6.78	0 0 0 0 0	0 0 0 0 0	✓				0.729 .878 .938 .988	0.87 - 1.0 .62 - .85 .61 - .78 .58 - .74	Shadowgraphs
CONFID. RM L57K14 Preflight jet and flight tests, PARD	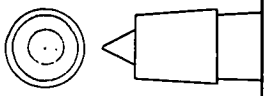	1 Isen-tropic	None	Sea level: 2.03 1.62 1.39 1.17 Flight: 0.80 to 1.90	Sea level: 7.70 6.13 5.27 4.44 Flight: 1.60 to 6.78	0 0 0 0 0	0 0 0 0 0	✓				0.729 .878 .938 .988	0.87 - 1.0 .62 - .85 .61 - .78 .58 - .74	Shadowgraphs
CONFID. RM L57K14 Preflight jet and flight tests, PARD	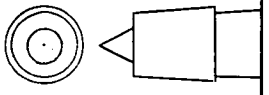	1 Isen-tropic	None	Sea level: 2.03 1.62 1.39 1.17 Flight: 0.80 to 1.90	Sea level: 7.70 6.13 5.27 4.44 Flight: 1.60 to 6.78	0 0 0 0 0	0 0 0 0 0	✓				0.729 .878 .938 .988	0.87 - 1.0 .62 - .85 .61 - .78 .58 - .74	Shadowgraphs

Bibliography

These strips are provided for the convenience of the reader and can be removed from this report to compile a bibliography of NACA inlet reports. This page is being added only to inlet reports and is on a trial basis.

CONFIDENTIAL

CONFIDENTIAL

CONFIDENTIAL

CONFIDENTIAL